POLITECNICO DI TORINO

Master's Degree in Aerospace Engineering

Master's Degree Thesis

Simulation of Blade-Tip Timing signals in Turbomachinery

Supervisors
Prof. Daniele Botto
Prof. Alain Batailly

Candidate
Marta Leoni

In collaboration with

A.a. 2021-2022
Graduation session April 2023

A mia sorella Angela ed alla sua Polo a righe con cui questa avventura ha avuto inizio.

Abstract

The bladed disks in aircraft engines are subject to vibration during operation, excitations shorten their lifespan and raise the possibility of crack formation, both of which can result in catastrophic damages. The conventional method for vibration measurement on turbomachinery blades is to apply strain gauges on the blade surface. In recent years, a non-intrusive alternative technique for measuring blade vibration using a non-contact method has gained popularity.

The Blade-Tip Timing (BTT) technique works based on the concept of time of arrival (TOA) of the blades passing in front of stationary sensors, placed on the casing around the blades. In absence of any structural vibration, the TOA would depend only on the rotational speed of the blade. Meanwhile, when the tip of the blade is vibrating, the TOA will depend on the amplitude, frequency, and phase of vibration. Hence, it is possible to associate these data to the vibration amplitudes and thus study the vibratory behavior of the blades. The application and the type of data that are required determine the number, type, and locations of the probes. The starting point of this research is to achieve a numerical simulation of Blade-Tip Timing measures to avoid the experimental constraints associated with this method and evaluate the blade-tip timing data processing algorithms. The Vibration and Acoustic Analysis Laboratory of the "Ecole Polytechnique de Montréal" has drawn up a Python code based on the principle of time integration and has been written to be able to simulate the amplitude of blade vibrations in a linear and non-linear framework. One of the new themes of the laboratory is to generate BTT signals, *i.e.* to digitally simulate the measurement of the vibration amplitude by a sensor to be able to study more precisely the characteristics of these signals. In the first instance, generate "tip timing" signals from linear vibratory signals obtained in the laboratory, drawing attention to possible improvements in the TOA computation. Subsequently, analysis algorithms dedicated to signal reconstruction were implemented and validated.

Key words: Blade-Tip Timing, Bladed disk, Vibration parameters identification, Blade arrival time.

Acknowledgements

I want to express my deepest gratitude to my supervisor, Professor Daniele Botto, for instilling a strong interest in me during his course of study and, subsequently, for allowing me to have this wonderful experience that led to the development of this project. A special thanks to Alain Batailly for his supervision during my time in Canada.

I can never thank my large family enough for supporting me at every moment despite being far from home. To my sisters and my brother, who are and will always be my reference points, and to my nephew, whom I hope to instill the possibility of achieving any goal.

Following my second family in Turin, without whom, I would have been completely lost in these years. An infinite thanks to everyone I left behind in Rome, especially my crazy girls from Ciampino, who never left me alone and welcomed me with open arms every time I returned home.

Thanks to those who accompanied me during the dance lessons that distinguished my university path.

Thanks to Emanuele, with whom I shared a good part of this adventure and to whom I owe everything for giving me the strength in the most difficult moments to move forward with my head held high.

Last but not least, I thank Ludovica, who, in 6 months, has proven to be a life partner that I will never forget.

Contents

List of Figures

List of Tables

Acronyms

BTT Blade Tip Timing

TOA Time of arrival

ND Nodal Diameter

EO Engine Order

TW Traveling Wave

OPR One Per Revolution

SPP Single Parameter Plot

TPP Two Parameter Plot

Chapter 1

Introduction

Aircraft must be equipped with a propulsion system to ensure sustenance and advancement in operational conditions. Consequently, the vast majority of aircraft are fitted with turboprop or turbojet engines. The common characteristic of such turbomachines is the presence of bladed disks, both in the fan, in the high and low-pressure compressor, and in the turbine. The primary goal of turbomachinery blade design is to increase turbomachine efficiency to reduce fuel consumption. To this end, blade design procedures focus mainly on the aerodynamic performance of blades. Indeed, bladed assemblies are subjected to several excitation sources, leading to forced vibration responses that may occur at or near a blade's natural frequencies. Severe vibratory loads may cause cracks, blade failures, and in the end, the total failure of the engine. Such vibrations can result from multiple factors; for instance, some of them, classified as non-linear vibrations, are due to interactions between the blades and the casing. As mentioned above, to reduce engine loss efficiency, during the design phase, one of the key objectives is to minimize the clearance between the tip of the blades and the engine casing because if it is too large, it causes disturbed airflow. However, in flight, the casing and blades will deform due to thermal expansion and different forces on the casing and blades. Hence, if this clearance is too small, contact between the blades and the casing is favored, and the blades start to vibrate due to the contact. The other part of the vibrations is due to the disturbance of the flow upstream of the blades by the presence of stator blades. This type of vibration is called linear vibration and can be destructive when the vibration frequencies reach the natural frequencies of the blade disk. Therefore, monitoring blade vibrations is of great importance. It prevents damage, and it is possible to predict the durability and the life of blades under operating conditions, and for this purpose, most engine manufacturers develop measuring techniques.

The techniques used for evaluating the vibration parameters of bladed assemblies can be classified into two types: contact methods and non-contact methods:

1. Two principal transducers are used in contact methods: strain gauges and accelerometers.

2. The non-intrusive method involves using sensors placed on the casing to calculate the passage time of the blade under them.

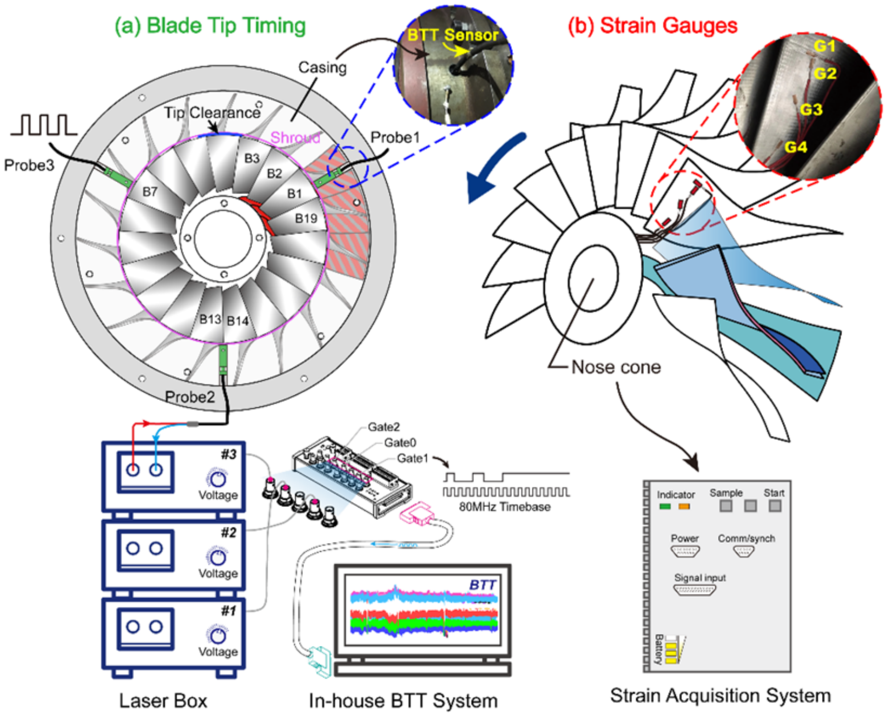

Figure 1.1. Measurement techniques

Strain gauges are the most commonly used technique employed in rotating blade vibration measurement. They have the advantage of high accuracy and well-established signal-processing algorithms. Nevertheless, both contact methods require work with radio telemetry or slip rings for data transmission. For this reason, there are design complications regarding the available space for the installation of the transducers, so they cannot be positioned on all the blades of a rotating disk. This is one of the main drawbacks of contact methods. Moreover, suppose the size of the transducer is not negligible concerning the component on which it is installed. In that case, its influence on the dynamic behavior of the element leads to inaccurate measurements. Furthermore, in harsh conditions, *e.g.* high temperature, the accuracy of strain gauges decreases drastically, so in such cases, they can be used only for estimating the oscillation frequency.

Meanwhile, **BTT** is an established technology that allows assessing all blades in an assembly. The development of new systems for measuring blade vibrations arose from the need to obtain other results, such as No influence on the dynamic behavior of the system, good accuracy in harsh conditions, and avoiding sensor damage through stationary probes. Since the BTT system appears capable of overcoming, at least partially, all of these issues, a great deal of research is being conducted on this technique. However, this assessment is restricted to modes showing a remarkable tip deflection and comes with difficulties in post-processing the heavily under-sampled BTT data. However, also in this case, there are some drawbacks:

- The quality of results depends on the probe positioning
- Difficulties in the post-processing of the heavily under-sampled BTT data.

1.1 Thesis outline

The structure of the thesis is presented here, with a brief description for each chapter:

- **Chapter 2: Literature Review**
  It describes the basic theory of the vibration of blades and disks. This chapter also presents the features of the BTT system, including the working principle, the instruments usually employed, and a few analysis techniques.

- **Chapter 3: Description and analysis of existing lab code**
  This chapter discusses the basic Python code present in the Montreal Polytechnique Vibration and Acoustics Laboratory.

- **Chapter 4: Numerical simulation development**
  This chapter develops the code for generating the BTT signals and optimizing the algorithm for obtaining the TOA.

- **Chapter 5: Simulation results**
  This chapter discusses the results obtained from the various simulations.

- **Chapter 6: Conclusions**
  This chapter summarizes the project, explains the limitations, and presents future developments.

Chapter 2

Literature review

2.1 Vibrations characterizing bladed disks

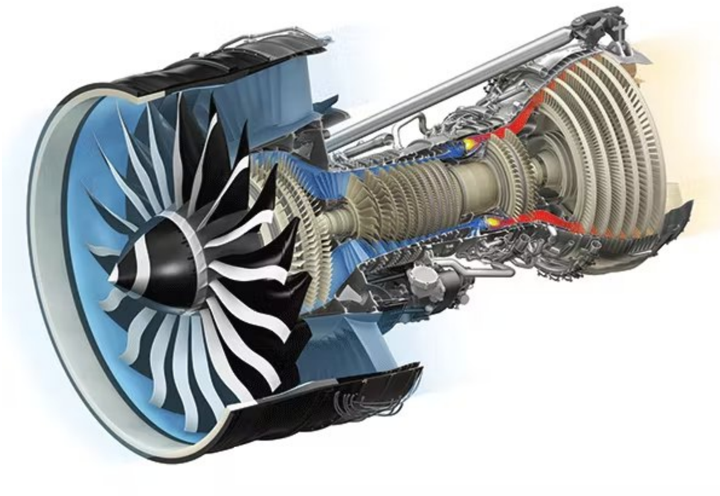

Figure 2.1. Cross-section of The GEnx turbofan engine (credit: GE [1])

The gas turbine is one of the most widely used propulsion systems for modern aircraft engines. The engine's core—the compressor, burner, and turbine—is also known as the gas generator since the output is hot exhaust gas. The compressor and turbine are defined as the turbomachinery, where the energy is added or extracted from the continuous flow by rotating blades' dynamic and aerodynamic action.

The numerous stages that make up the compressor and turbine consist of bladed disks, which are the main components, and these consist of a disk and several blades that are fixed around the disk, as shown in figure 2.2. The movement of the blades can be broken down into two parts: the overall rotation around its axis and the vibrations of the blade disk.

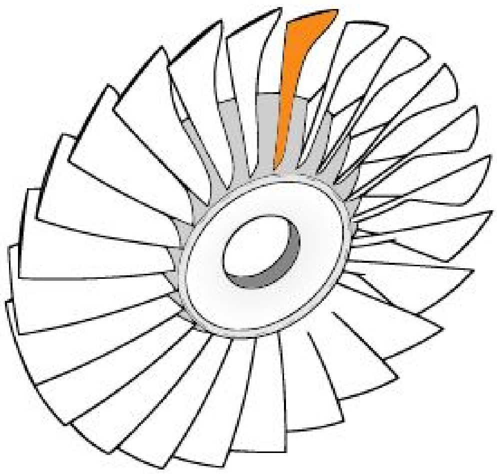

Figure 2.2. Bladed disk

Under normal operating conditions, the vibrations of a bladed wheel are linear, mainly due to the variation of aerodynamic load on the blades due to the presence of fixed blades upstream of the flow. The associated excitation frequency is thus dependent on the number of blades in the rectifier and the rotational speed of the impeller. In addition, blade disk vibrations can also be non-linear due to friction, slippage, and contact where relative movement is allowed between components. [8]

2.1.1 Modal analysis

In turbomachines for aeronautical and aerospace applications, the rotors clamped on the rotating shafts are elastic elements and are not infinitely rigid. Therefore, the dynamic analysis of these components is very demanding for the structural designer, who must avoid resonance conditions within the machine's operating range or control the vibration amplitude by introducing additional damping into the system. Therefore, dynamic analysis necessarily starts with a modal system analysis to identify its natural frequencies and proper modes.

Blade Modes The blade can vibrate in three directions that are radial, tangential and axial directions. The blade vibration modes are mainly characterized by bending and torsion movements. It should be noted that the shape of a blade is too complex to be able to study it as a simple beam, in fact blades have the following features that make their structural analysis more difficult:

- The cross-section is not constant but tapered
- The blade is twisted along the principal axis to avoid aerodynamic problems
- The cross-section has a non-regular shape for aerodynamic efficiency

The listed features imply that the flexural and torsional mode shapes are often combined. For this reason, the only way to perform a dynamic structural analysis is by using a finite element model from which it is possible to extract the modal shapes.

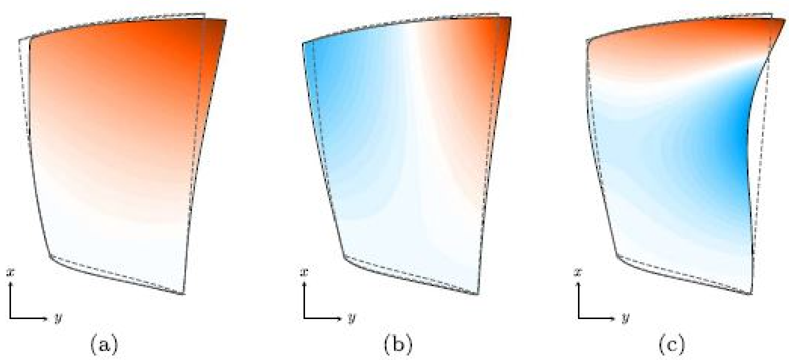

Figure 2.3. First three normal modes of the reference blade: (a) first bending mode (1B), (b) first torsion mode (1T), and (c) second bending mode (2B) [2].

Finite-element schematization takes advantage of numerical computational techniques through which the dynamic behavior of mechanical systems can be described using ordinary differential equations, which are much less complex than the partial differential equations that describe continuous systems instead. In figure 2.3, there are some examples. Rotating blades are subjected to loads that influence their dynamic behavior, and the main variables which affect the values of natural frequencies are centrifugal force, temperature, and the presence of cracks. The centrifugal force causes an increase in the natural frequencies; this phenomenon is called the stiffening effect, with some corresponding changes in the mode shapes. The temperature, instead always has a de-stiffening effect as it increases. While as for the presence of cracks, It has a de-stiffening effect on the dynamics of blades.

Disk Modes The disk vibration is characterized by circumferential and axial sinusoidal displacements, in which nodal points form concentric nodal circles and radial lines called nodal diameters.

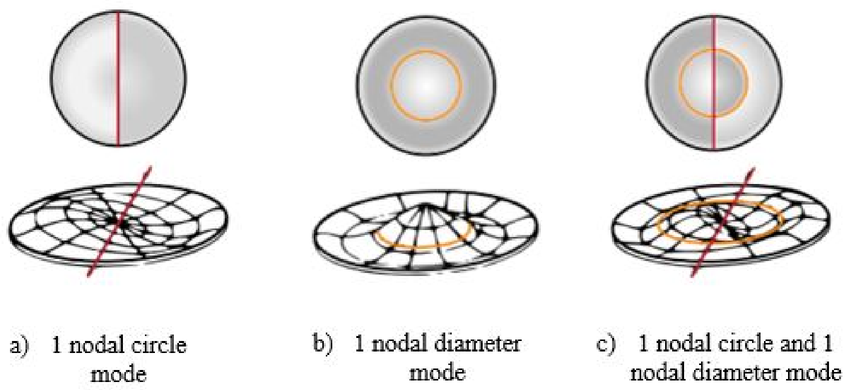

Figure 2.4. Vibration modes of a disk

A nodal diameter is the set of points on a disk's diameter that does not vibrate, and these diameters exist only in pairs. A nodal circle is a set of points on a process disk that does not vibrate. The number of nodal diameters and circles indicates the mode at which the disk is vibrating. Some vibration modes are called dual modes, meaning that two vibration modes can be excited about the same excitation frequency. These modes are generally orthogonal and can be manifested by the appearance of a Progressive Wave (PW), also called "Traveling Wave" (TW), in the direction of rotation of the impeller or the opposite direction [8]. Combinations of nodal circles and nodal diameters result in complex shapes, as shown in figure 2.4.

When blades are fitted to a disk, this phenomenon persists and becomes more apparent, because blades are often much less stiff than the disk on which they are fixed. That's because the disk cannot be considered perfectly rigid in most cases. In such situations, the dynamic analysis of a single blade doesn't lead to accurate results, which can be extended to the assembly behavior. Thus an analysis of the whole disk is necessary. The number of nodal diameters and circles rises with speed with a limit determined by the number of blades [9].

$$\begin{aligned} ND_{max} &= \frac{N_{blades}}{2} \quad \text{for an even number of blades} \\ ND_{max} &= \frac{N_{blades-1}}{2} \quad \text{for an odd number of blades} \end{aligned} \tag{2.1}$$

2.1.2 Vibrations characteristics

Synchronous vibrations When the vibration is synchronous, the same points of the response waveform of the blade tip are measured revolution after revolution. So standard frequency analysis techniques are not effective. The following relationship gives the Engine Order (EO):

$$EO = \frac{\omega}{\Omega} \tag{2.2}$$

where ω is the blade vibration frequency in rad/s and Ω is the assembly rotational speed in rad/s.

Asynchronous vibrations Asynchronous vibration, on the other hand, occurs when the blade vibration frequency is not an integer multiple of the rotor speed.

Asynchronous resonances are mainly due to aerodynamic instabilities such as rotating stall and flutter [10].

2.1.3 Type of vibrations

In a physical system, two classes of vibrations can generally be distinguished: **free** and **forced** vibrations.

Free vibrations occur when a system oscillates under the action of forces inherent in the system and the absence of external forcings. Once subjected to an initial perturbation, the system will vibrate at one or more of its natural frequencies, which are properties of the dynamic system determined by the distribution of its mass and stiffness. A combination of the principal modes will give the resultant motion and continue indefinitely without damping.

The study of free vibration provides information about the dynamic properties of the system, which are used to evaluate its response when subjected to the action of one or more time-varying forcings.

Forced vibrations occur in the presence of time-varying forcings and possess the same frequency as excitation. It should be noted that should this coincide with one of the system's natural frequencies, a resonance condition will occur. This phenomenon is such that the oscillations reach higher and higher amplitudes that can be limited only by the presence of the damping factor.

Forced vibrations in a linear context A system is defined as linear if its response to a linear combination of input signals equals the same linear combination of the individual responses to each input signal. Under normal operating conditions, the vibrations of the impellers are linear. Aerodynamic loads are the main cause of these vibrations, in particular, due to the presence of rectifiers. These are exploited to recover some of the lost energy due to the velocity component that does not contribute to engine operation. To improve the aerodynamic efficiency of turbo-shaft engines, static rectifiers, also consisting of blades, are placed upstream and downstream of the impellers. However, these rectifiers' local presence perturbs the flow, inducing a load change on the downstream blades, which vibrate. [8]

Forced vibrations in a non-linear context Turbomachines have many non-linear interfaces associated with contact or friction. Each has led to the development of specific methodologies for their analysis. [11] Some of them are highlighted in Figure 2.5 .

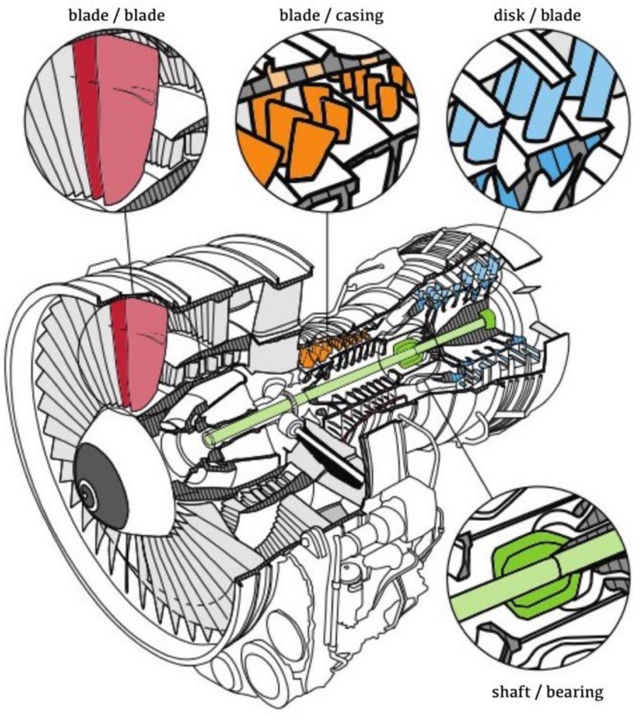

Figure 2.5. Main contact interfaces in a turbomachine.

Non-linear vibrations can also occur in the accidental configuration when the design's clearance is insufficient to avoid interaction between the fixed and rotating parts. In the absence of a unified theoretical framework for analyzing non-linear mechanical systems, the strategy adopted by the industry to better understand the vibratory phenomena associated with each interface is based on collaborations with university laboratories to develop *ad-hoc* numerical tools, adapted to their needs, exceeding the capabilities of commercial calculation codes [11].

2.2 Blade tip timing measurement method

A Blade Tip-Timing signal is a signal whose purpose is to measure the amplitude of vibration of the tip of the blades of a bladed disk. The idea is to place sensors detecting the passage of the tip of a blade on the engine casing at different points around the circumference of the blade wheel to measure the time of arrival (TOA) of each blade. When the blades are not vibrating, each blade passes a sensor at a regular time interval if the impeller rotation frequency is constant. When the blades are vibrating, this arrival time differs due to the vibration amplitude. From this time difference, and thanks to the rotation frequency of the motor obtained with an OPR (One Pulse per Revolution) sensor, the amplitude of the blades can be deduced. The various sensors, together with signal processing algorithms, can thus be used to determine the amplitude and vibration frequencies of the blades. If sensors are now placed at the leading and trailing edges of the blades, the different vibration modes can be deduced (bending, twisting, etc.).

2.2.1 Basis of the Method

Tip Timing measurements consist of three steps as follows [12]:

- Data acquisition
- Data post-processing
- Data Analysis

Two different pieces of time information are needed[13]:

1. Measured Time of Arrival TOA_{meas} : measured by a stationary optical or magnetic probe when a blade passes in front of it.
2. Expected TOA_{exp}: if there were no vibrations encountered

The difference Δt between the real and the expected TOA is then used to compute the displacement of the blade tip concerning its nonvibrating configuration, knowing the disk's radius and its rotational speed. This is carried out to analyze them and identify the frequency and amplitude of vibration. The expected ToA can be estimated using one of the two procedures listed below:

- Using the Once per Revolution (OPR) sensor;
- Using the central time computed from the ToA of multiple blades on a selected probe.

In a conventional BTT acquisition system, the housing and the shaft are instrumented, as shown in figure 2.6.

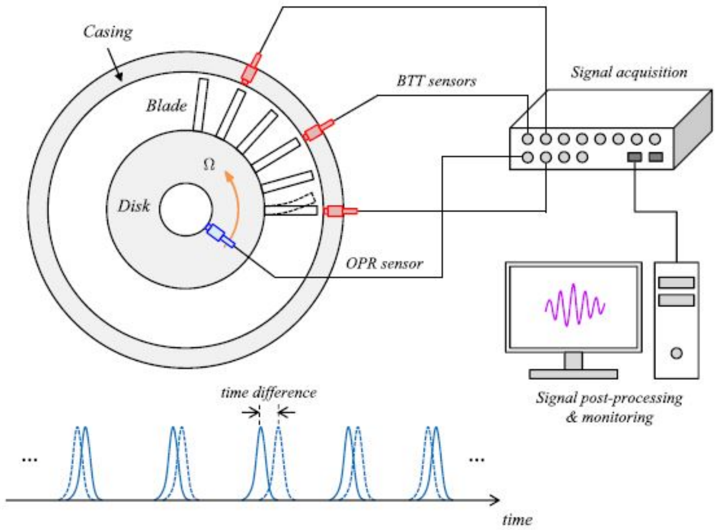

Figure 2.6. Schematic illustration of a BTT measurement system [3].

The sensor connected to the shaft of the OPR type provides knowledge of the actual rotational speed of the rotor, which experimentally exhibits some variability from the desired speed [14]. Whereas the sensors connected to the casing provide a raw signal, usually analog, which is then translated into a pulse corresponding to the passage of a blade [15].

As mentioned above, the principle of operation of the BTT measurements is based on comparing blade passage times in front of sensors, in the case with and without vibrations. This time of passage is called the Time Of Arrival. If M sensors are used, they are numbered from 1 to M. The position of a sensor p is defined by its angular position θ_p on the circle representing the casing, as shown in figure 2.6. For an impeller with N blades, each blade is numbered from 1 to N. Thus, the angular position of a blade j is defined by:

$$\theta_j = j\frac{2\pi}{N} \tag{2.3}$$

TOA expected If the bladed disk rotates at a constant rotational frequency and the blades do not vibrate, each blade passes in front of a sensor at a regular time interval. Hence, this time is determined theoretically from the rotation frequency of the blade disk. The rotation frequency is measured by the OPR, which provides a pulse per revolution of the impeller. In particular, for a bladed disk rotating in the trigonometric direction and with an initial angular position of the blade j lower than the angular position of the sensor p, the passage time of a blade j in front of a sensor p is defined by [16]:

$$t_p^{k,j} = \frac{\theta_p - \theta_j + 2k\pi}{\Omega} \tag{2.4}$$

where k is the number of revolutions of the impeller.

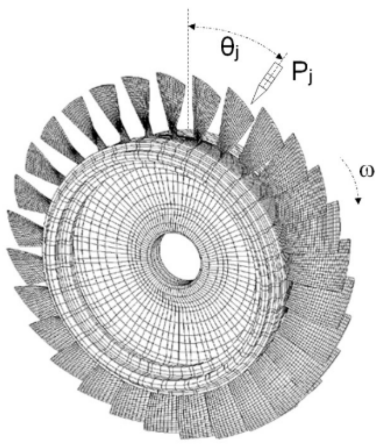

Figure 2.7. Schematization TOA_{exp} obtainment.

Analogously, this TOA_{exp} can be determined when the blade disk's rotation direction is clockwise and when the initial angular position of the blade is greater than the angular position of the sensor.

Once the transit times are obtained in the case with and without vibration, $t_p^{k,j}$ and $t_{v,p}^{k,j}$ respectively, and thanks to the rotation frequency Ω obtained with the OPR sensor, the amplitude of the blades j, measured by sensor p at k rpm can be deduced through the formula 2.5.

$$a_{k,p}^{j} = h_{blade}\Omega(t_p^{k,j} - t_{v,p}^{k,j}) \tag{2.5}$$

where h_{blade} is the blades' height. This measured amplitude represents the distance traveled by the blade tip based on the transit time difference between the case with and without vibration.

2.3 Probes

Different non-contact measurement methods can be used, depending on the physical mechanisms and the conditions in which the sensors operate. Different sensors can be used for Blade Tip Timing measurements, including inductive, eddy-current, microwave, optical, and capacitance sensors. Here is a detailed comparison of these sensors:

- Inductive sensors: Inductive sensors are simple in design, low cost, and have a long life. They are optimal for embedded systems. However, they have limited bandwidth and can be affected by electromagnetic interference.
- Eddy-current sensors: Eddy-current sensors are also non-contact sensors that can measure blade vibrations. They have high bandwidth and can be used in high-temperature environments. However, they are sensitive to the distance between the sensor and the blade, and their accuracy decreases as the distance increases.
- Microwave sensors: Microwave sensors have a large bandwidth and are not

sensitive to pollutants, making them promising for BTT measurement. They are suitable for high-temperature environments and are non-intrusive. However, they require complex signal-processing algorithms.

- Optical sensors: Optical sensors are also suitable for BTT measurement. They have high accuracy and large bandwidth. However, they are unsuitable for high-temperature environments and require line-of-sight.
- Capacitance sensors: Capacitance sensors are also suitable for high-temperature environments. They have high accuracy and large bandwidth. However, they can be affected by electromagnetic interference.

Inductive sensors Inductive sensors for BTT measurements work on the principle of electromagnetic induction. An inductive sensor consists of a coil that generates a magnetic field. When a metallic object, such as a blade, enters the magnetic field, eddy currents are induced in the object. These eddy currents generate a secondary magnetic field that opposes the primary magnetic field of the sensor. The change in the primary magnetic field is detected by the sensor and converted into an electrical signal. This signal corresponds to the position of the blade tip as it passes through the sensor's magnetic field. The sensing range and output of an inductive proximity sensor depend on the type of metal being detected, and it is used for positioning and detecting metal objects. Inductive sensors are commonly used for BTT measurements due to their simple design, low cost, and long life [17], [18].

Eddy-current sensors Eddy-current sensors for Blade Tip Timing (BTT) measurements engage the principle of electromagnetic induction. An eddy-current sensor consists of a coil that generates a varying magnetic field. As a blade passes through the sensor's magnetic field, eddy currents are induced. [19]The eddy currents generate a secondary magnetic field that opposes the primary magnetic field of the sensor. The change in the primary magnetic field is detected by the sensor and converted into an electrical signal. This signal corresponds to the position of the blade tip as it passes through the sensor's field. The effect of tip clearance, blade geometry, and blade velocity on the output of the eddy current sensor can be simulated to calibrate and estimate the conductor time. Eddy-current sensors are commonly used for BTT measurements due to their high accuracy and sensitivity [20].

Microwave sensors Microwave sensors work on microwave reflection or transmission principles. A microwave sensor consists of a transmitter that generates microwave signals and a receiver that detects the reflected or transmitted signals. As the blade passes through the sensor's microwave field, it causes a change in the reflected or transmitted signal. This change corresponds to the position of the blade tip as it passes through the sensor's field. The reflected or transmitted signal is then processed to determine the TOA of the blade tip. Microwave sensors have a large bandwidth and are not sensitive to pollutants, making them promising for BTT measurement. They are suitable for high-temperature environments and are non-intrusive. However, they require complex signal processing algorithms. A microwave BTT system using a patch antenna-based sensor has been introduced, which can measure BTT and tip clearance at the same time. The system filters, down-converts, and processes the received microwave signal to generate IF signals sampled for tip clearance measurement. The acquired timing pulse signals are calculated to find the TOAs of all blades and uploaded to the host [18].

Optical sensors As for Optical sensors, they are based on the principle of light reflection or transmission. An optical sensor consists of a light source and a receiver. The light source emits a beam of light reflected or transmitted by a blade passing through it. The receiver detects the reflected or transmitted light, and the change in the light intensity is converted into an electrical signal.[21] This signal corresponds to the position of the blade tip as it passes through the sensor's field. Optical sensors have high accuracy and large bandwidth. However, they are unsuitable for high-temperature environments and require line-of-sight. Capacitance sensors are also commonly used for BTT measurements, which work based on changes in capacitance between the blade tip and the sensor [22].

Capacitive sensors Capacitive sensors for BTT measurement operate using capacitance changes between the probe and blade tip. The capacitive sensor consists of a probe that generates an electric field. As a blade passes through the sensor's electric field, the capacitance between the blade tip and the sensor changes. The change in capacitance is detected by the sensor and converted into an electrical signal. This signal corresponds to the position of the blade tip as it passes through the sensor's field [23]. The capacitive sensor obtains blade arrival times by measuring the change in capacitance between the probe and the blade tip. Capacitive sensors have high accuracy and large bandwidth, but they can be affected by electromagnetic interference. Various compensation methods can be used to reduce interference effects and improve the accuracy of BTT measurements using capacitive sensors [24]. In summary, each type of sensor has its advantages and disadvantages, and the choice of the sensor depends on the specific requirements of the BTT measurement application.

2.4 Measurement techniques

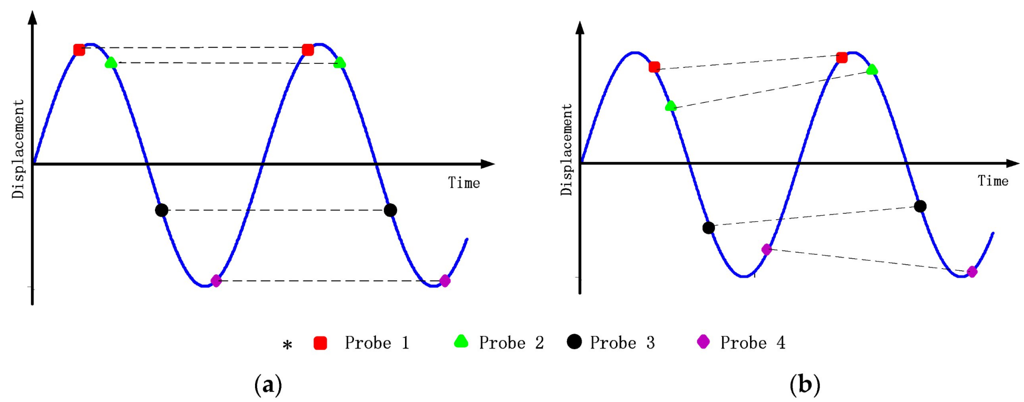

Figure 2.8. Vibration signal sampled by four optical sensors (a) synchronous vibration (b) asynchronous vibration [4].

Within the BTT method, several measurement techniques do not necessarily use the same number and angular positions of the transducer and do not provide the same vibration signal parameters. Depending on the vibration characteristics, some allow, for example, to reconstruct the signal, while others allow identifying the resonance. These measurement techniques differ mainly depending on whether the vibrations are synchronous or asynchronous. Figure 2.8 summarizes the difference between these two types of vibrations from a sensor perspective.

Concerning Synchronous vibrations, the vibration frequency of the blades is a multiple of the rotation frequency of the impeller. The difficulty in measuring synchronous vibrations lies in the fact that a sensor can only provide one data per blade: each time the blade passes in front of the sensor, the TOA measured is the same; this means that the acquisition is strongly aliased and an important consideration has to be made concerning the Nyquist sampling criterion: only the response components with a frequency less than half the rotation rate are defined uniquely, and all other frequency components are aliases. The challenge is to get more samples per revolution for each blade and reduce the aliasing. Hence, if the sensors are uniformly distributed along the circumference of the assembly, the sampling frequency is defined by [25]:

$$f_e = M\frac{2\pi}{\Omega} \tag{2.6}$$

Where M denotes the number of sensors used. The Nyquist-Shannon criterion defines that [26]:

$$f_e > 2f_{max} \tag{2.7}$$

Where f_{max} is the maximum frequency of the blade vibration signal. Therefore, the idea would be to place as many sensors as possible on the casing to increase the sampling frequency and get closer to the Nyquist frequency. That is because if this criterion is not satisfied, the signal is undersampled, which leads to aliasing of the spectrum, and the true signal cannot be reconstructed by conventional methods, as shown in figure 2.9

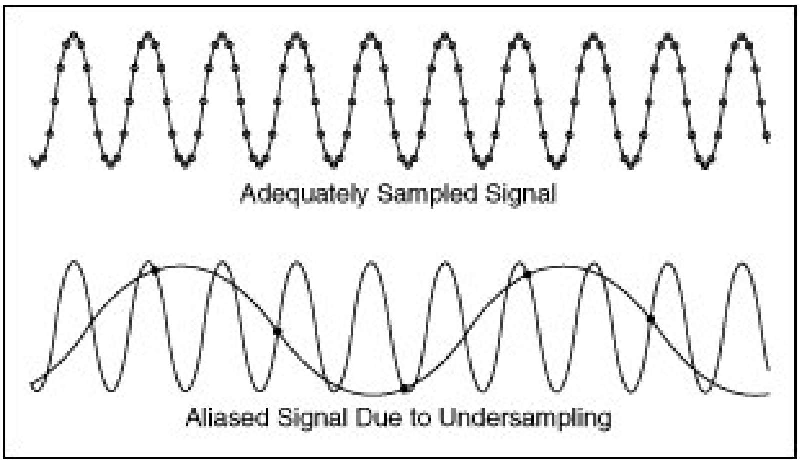

Figure 2.9. Aliased signal [5].

Unfortunately, blade vibration frequencies are generally too high and require too many sensors to be realistically implemented. Several methods have been developed to circumvent this problem, but they need prior knowledge of the assembly response, including Campbell's diagrams and EO. This knowledge is obtained through numerical models of the bladed disk.

2.4.1 Methods for analyzing synchronous responses

Different techniques have been developed over the years, and they can be divided into two main types: direct and indirect methods.

Direct method

Direct methods consist of measuring the instantaneous amplitude of vibration of the blades at a given speed of rotation of the assembly. These methods are mainly used to determine the characteristics of the resonance (especially the maximum amplitude) [10]. The main features of direct methods are briefly summed up in the following list:

- At least four probes are needed
- They work at a constant rotational speed of the assembly

- It is possible to determine the EO of the vibration

The most used are Circumferential Fourier Fit, the Global Autoregressive method, and the Determinant approach.

Least squares method The least squares method is used to predict the amplitude and phase of the resonance signal. Theoretically, this method requires two sensors. The idea is to minimize the sum of squares of the residuals, where the residual is the difference between the amplitude calculated by the BTT method and the adjusted amplitude after regression [13]. Increasing the number of sensors improves the accuracy of the output signal reconstruction concerning the real signal. However, this method requires prior knowledge of the blisk, especially the natural frequencies of the blades and the EO. This knowledge is usually obtained from finite element software. A disadvantage of this method is that it is partly based on a numerical model, which may not be fully representative [13]. In addition, this method is particularly affected by measurement noise. However, improvements have been proposed to overcome these constraints.

As already stated, the method of least squares is used to predict the amplitude of the resonance signal [10]. For linear vibrations, since most of the blade excitation signals are sinusoidal, the vibrational response of the blades is also sinusoidal, and it is, therefore, possible to reconstruct the signal. Assuming the steady state is reached, the tip response is assumed to be sinusoidal and mono-harmonic. Hence it can be expressed as follows [27]:

$$A \sin(\omega t + \phi) \tag{2.8}$$

When the excitation frequency ω is known, the goal is to determine the amplitude A and phase ϕ to reconstruct the signal fully. By placing a sensor p, it is possible to obtain the instantaneous vibration amplitude of a blade j:

$$a_p^j = A \sin(\omega t_{v,p}^j + \phi) = h_{blade}\Omega(t_p^j - t_{v,p}^j) \tag{2.9}$$

A system of second-order equations is obtained by placing two sensors to reconstruct the signal. It is important to note that the sensors are evenly distributed around the casing. Therefore, the number of sensors should not be a multiple of the excited EO so that the measured amplitude is not the same for all sensors [16].

Other least-squares-based methods allow reconstruction of more complex signals but require dedicated processing algorithms based on Fourier transforms.

Indirect method

Indirect analysis methods typically take one or two response samples from each assembly rotation as a synchronous assembly resonance is traversed. Therefore, they can only give a single frequency component, i.e., the resonant frequency. As the resonance is crossed, the excitation and response characteristics change due to changes in the assembly rotation speed [10]. The most used are the Single Parameter Plot method (SPP) and Two Parameter Plot method (2PP); they share the following features:

- Only one (in SPP) or two (in 2PP) probes are needed
- The assembly speed must change during the measurement

Single Parameter Plot The technique was developed for the first time in 1970 by Zablotsky, and Korostelev [28]; it is the most basic measurement technique as it involves measuring a single blade response parameter, such as the blade-tip displacement, using a single sensor positioned on the casing. The blade response is assumed to be assimilable to a damped forced harmonic oscillator with one degree of freedom. A sensor can only supply the observed amplitude and one datum per blade because the vibrations are synchronous. To avoid this constraint, the method requires the resonance to be excited by varying the assembly rotation speed so that the assembly is forced to traverse the resonance of interest. The form of the measured displacement versus rotational speed characteristic depends on the position of the measurement probe relative to the assembly forcing function [6]. Typical plots at different measurement positions for the same forcing term are

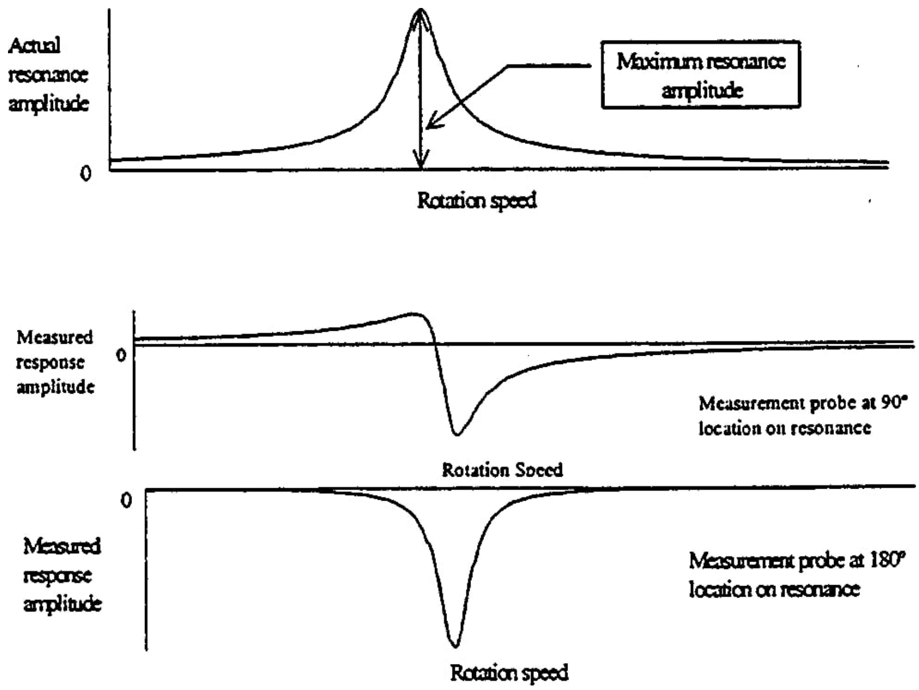

Figure 2.10. Comparison of actual and measured response amplitudes for different measurement position signal as a function of Ω [6].

shown in figure 2.10 The shape of the plots is affected by the probe position, but this does not pose a problem because the peak-to-peak amplitude determines the displacement amplitude in any situation. Once the amplitude of the vibration is known, the following parameter to be evaluated is the oscillation frequency ω. Up to now, the only known value related to it is Ω, but to obtain ω, it's necessary to understand the EO of the excitation. The only way to determine the EO associated with the observed synchronous vibration using a single sensor is to predict it from a FEM analysis, whose primary output, in this instance, is the Campbell diagram of the blade. It allows the identification of expected resonances at the intersection of the modal and Engine Order lines. As shown in figure 2.11, natural frequencies (blue lines) and excitant frequencies (red lines) are represented as a function of the rotation speed of the system.

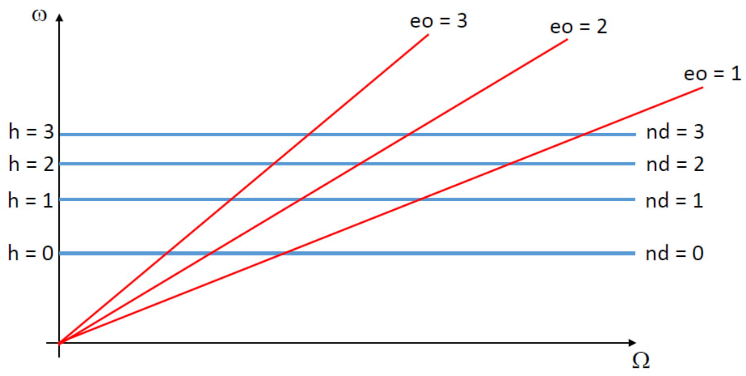

Figure 2.11. Example of a Campbell diagram

The Campbell Diagram is shown here concerning a modal family of a body comprising six sectors that are being stressed by a force that may be described as a linear combination of three engine orders [29].

, Unfortunately, this method has several disadvantages: the one degree of freedom oscillator assumption is valid for an isolated blade and not for an impeller. Additionally, this technique does not consider the fact that the blade can be excited in multiple modes. Several improvements have been proposed (S. Heath and M. Imregun [30]), mainly by replacing the one-degree-of-freedom system with a multiple-degree-of-freedom numerical system.

Two Parameter Plot The two-parameter method was developed from observing two measurements of a synchronous resonance from probes on the same axial position on the assembly casing [6]. Initially, this method also assumes that the vibrations have the shape of a one-degree-of-freedom oscillator. The two sensors will measure the same signal at two different points. Considering two probes, where probe A is located before probe B in the direction of assembly rotation and angular measurements are positive in the direction of rotation, given that the assembly vibration response displacement amplitude at the probes x_A and x_B can be calculated from the timing measurements. For a synchronous resonance of order

n, x_A, and x_B are equal to:

$$
\begin{aligned}
x_A &= A \cos n\Omega t_A + \psi = A \cos n\theta_A + \psi \\
x_B &= A \cos n\Omega t_B + \psi = A \cos n\theta_A + \psi + n\Delta\theta
\end{aligned}
\tag{2.10}
$$

where:

- A, ψ are the amplitude and phase of the assembly response
- $\Delta\psi$ is called Spacing on the Resonance (PSR)
- $\Delta\psi = n\Delta\theta$ is the angular separation of the measurements on the resonance
- $\Delta\theta = \theta_B - \theta_A$ is the angular spacing between probes A and B

An ellipse is obtained by varying the excitation frequency and displaying the measured amplitudes in parametric coordinates. The ratio of the minor axis to the ellipse's major axis is used to determine the value of the PSR.

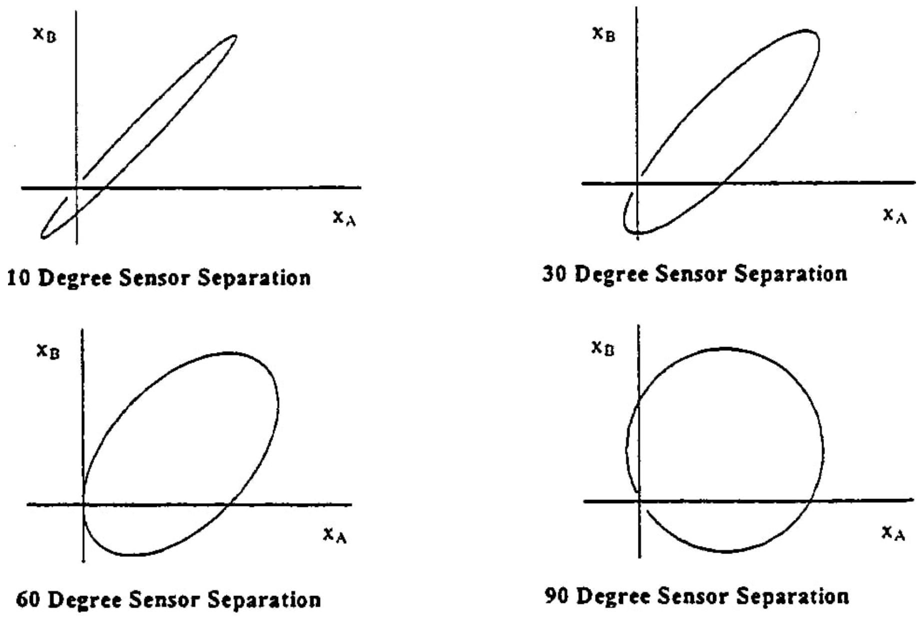

Figure 2.12. Plots of x_A versus x_A for different probe spacing [6]

Figure 2.12 shows the display in parametric coordinates of the measured amplitudes for different distances between sensors at resonance. The resonance order, n, can be calculated from:

$$n = \frac{\Delta\psi}{\Delta\theta} \tag{2.11}$$

However, one source of error in this method is that the vibration amplitude is assumed to be constant, as the excitation frequency varies when the amplitude changes as the excitation frequency varies. This is not a problem for small vibration amplitudes, but as the amplitudes increase, the error becomes more significant [31].

2.4.2 Methods for analyzing asynchronous responses

Asynchronous response analysis methods aim to identify the amplitude and frequency of non-integral order assembly resonances measured at the blade tips. There is no such problem with the sensors' single data for asynchronous vibrations. Still, the undersampling problem exists but can be more easily circumvented because the TOA measured at each revolution for a blade is different. The frequency components of the tip displacement are usually extracted by the Fourier transform, providing the amplitude and frequency of the blade tip oscillations through a single-blade or all-blade spectrum.

Single-blade spectrum Several methods are available for identifying resonance frequencies from a Fourier analysis of the response parameters. The frequency identification using tip-timing analysis methods is difficult because the value is determined indirectly from the single and all blade spectra. Analysis of individual blade spectra aims to identify the proper response frequency components for the aliased frequency components in the unique blade spectrum. A fundamental requirement of the analysis method is that the aliased frequency components are distinct. Considering that the frequency of an asynchronous response is not an integer multiple of Ω, the phase of the response samples will be different on successive rotations. Still, as the sampling frequency approaches an integer multiple of the response frequency, the change in measured response on subsequent rotations will be small. The overall response amplitude, which could contain more frequency components, is the difference between the maximum and minimum response amplitudes. The maximum frequency in the single blade spectrum is half the assembly rotation frequency such that most resonances are present as aliases in the spectrum [10]. Individual blade spectra have a low signal-to-noise ratio due to aliasing all response frequency components into a limited number of discrete frequency points. Therefore, the noise level cannot be reduced as response bandwidth cannot be limited before sampling. One advantage of the analysis method is that it gives the resonant response amplitude for each blade [32].

All-blade spectrum This method assumes that the impeller vibrates in modes comprising nodal diameters (existing in pairs), the set of points where the vibration amplitude is zero. When the bladed disk is rotating, the displacement of the nodal diameters can be assimilated to a progressive wave that moves in the same or opposite direction to the rotation of the impeller. Analysis of the all-blade spectrum aims to identify the nodal diameter mode associated with the resonant frequency components in the all-blade spectrum [32]. Indeed, if we assume that the blades vibrate at the same frequency, it is possible to measure the successive amplitude of each blade and thus to have the response of the progressive wave. The advantage of this method is that the sampling frequency is equal to the number of blades multiplied by the rotation frequency, which allows relatively high sampling frequencies compared to other methods and, therefore, avoids spectrum aliasing. This technique initially uses one sensor, but Watkins and Chi have proposed an improvement using two sensors. The standard Fourier analysis techniques assume a constant time step between samples, but of course, this happens only in the blades' absence of vibrations and mistuning. Thus the spectra are subjected to errors that produce some additional frequency components.

Chapter 3

Description and analysis of existing lab code

Currently, at the Polytechnique Montréal laboratory, a Python language code based on the principle of temporal integration has been developed to numerically simulate the vibration amplitude of blades in both linear and nonlinear regimes and, in this regard, evaluate blade/casing interactions. In addition, one of the new topics in the lab is the generation of BTT signals, thus the digital simulation of vibration amplitude measurement by a sensor to study the characteristics of these signals more accurately.

3.1 Description of the time integration module

To numerically simulate the passage of blades in front of a sensor, relying on some temporal integration code output parameters is necessary. The latter consists of a numerical simulation of the rotation of the impeller for a given period. This duration is divided into small intervals equal to a previously defined time step. The idea is to calculate the blade displacement parameters at each multiple of this time step up to the simulation duration, using the value of the previous blade parameters. For example, an impeller model has a certain number of blades, called sectors, and each blade tip consists of several nodes. Precisely, the displacement parameters of the blade at each of these nodes and the constraints on each of the elements associated with the nodes are calculated. In particular, each blade tip node's radial, tangential, and axial displacement can be obtained. The model studied here is NASA rotor 37 illustrated in figure 3.1.

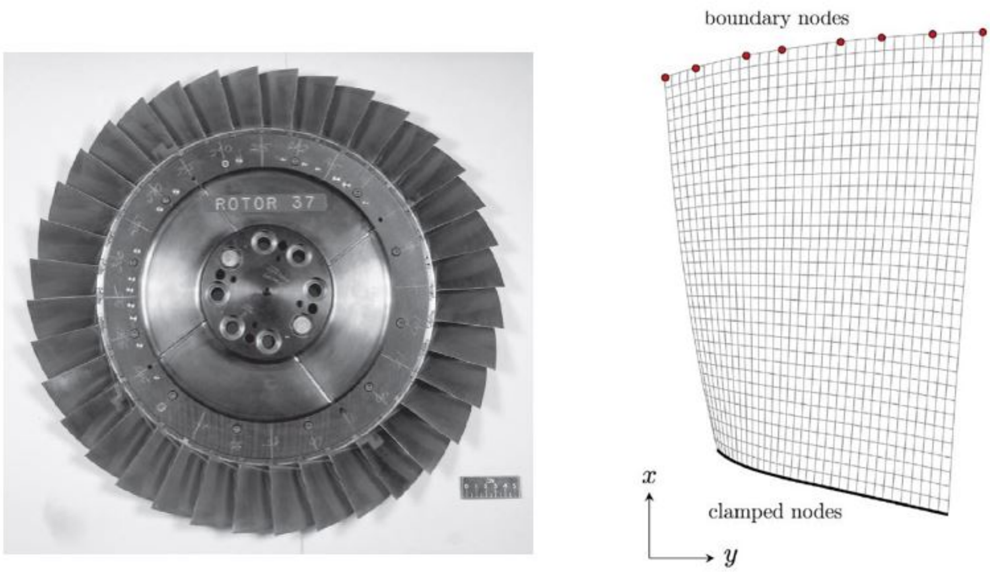

Figure 3.1. Picture of NASA rotor 37 [7] and Finite element mesh of the single blade [2]

It is a transonic axial flow compressor composed of 36 blades initially designed and tested at NASA's Lewis Research Center in the late 1970s. Nevertheless, the numerical model has only one blade whose tip is divided into eight nodes, numbered from 0 to 7. This is because blade mistuning is not studied here, and the single-blade model significantly reduces the computational time during simulations without changing the behavior of a tuned Bladed disk.

3.2 Blade tip-timing signal generation program

The aim is to determine the parameters underlying the Blade Tip Timing measurement technique, specifically the Time of Arrival (TOA) of the blade in front of one or more sensors, both when it is vibrating and when it is not, in detail TOA_{meas} and TOA_{exp}. This involves simulating the presence of a sensor that measures the times when the vibrating blade passes through, transforming the continuous amplitude signal at the end of a blade into a sensor-provided call. This information is then integrated into the time integration part of the program. Additionally, vibration-free transit times are calculated using the blade's initial position and the sensor's angular position.

Input parameters It is necessary to place the sensor along the tangential and axial directions. Therefore, the input parameters are as follows:

- **Angular position of the sensor:** this value is between 0 and 2π.
- **Nodal position of the sensor:** This value is one of the node numbers of the blade.

The nodal position of the sensor corresponds to the node of the blade above which the sensor is placed. Multiple sensors can be placed at the same time for different node positions and different angular positions. The blade is excited by a sinusoidal force, the application points of which are the nodes at the blade's tip. This type of force simulates aerodynamic loading, and the resulting vibrations are linear. The response of the blade at each node is, therefore, sinusoidal. According to equation 2.5, the difference of TOA between the case with and without vibrations is proportional to the amplitude of the measured vibrations. During the computation of time differences, various parameters can be varied, and the evolution of the TOA difference can be observed to ensure the algorithm's validity.

Chapter 4

Numerical code development

4.1 Signal captured from the numerical probe

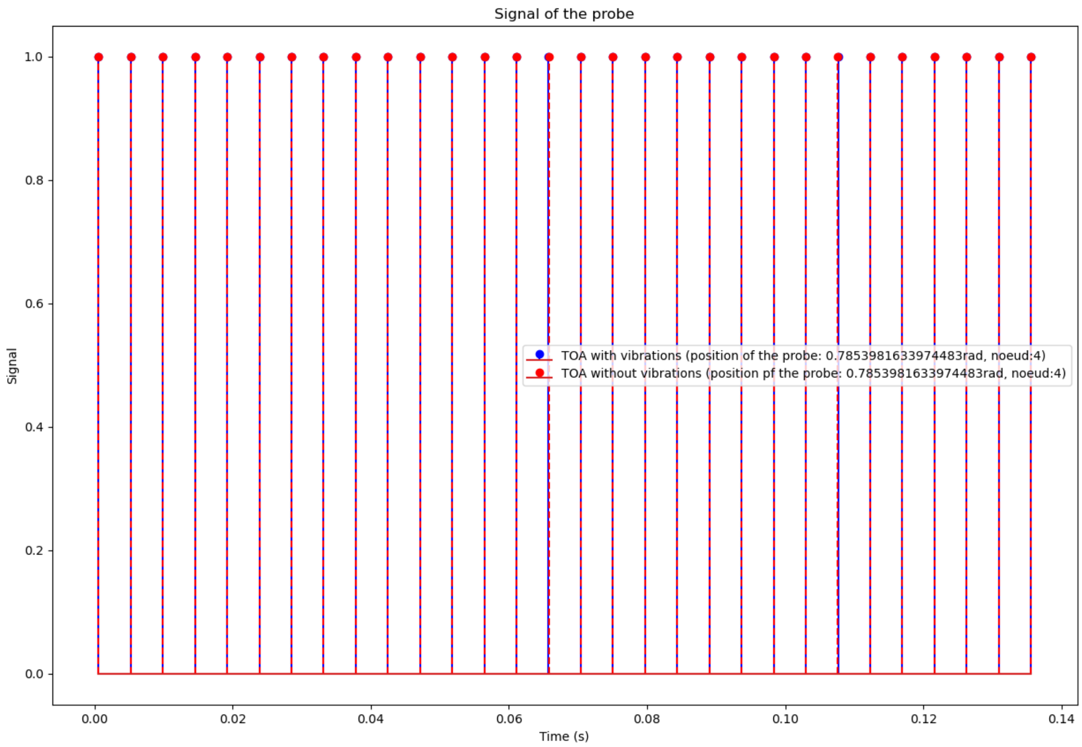

Figure 4.1. Sensor signal versus time for an excitation frequency of 750 Hz and a sensor angular position at $\frac{\pi}{4}$ rad

It is assumed that the numerically simulated sensor is perfect; in fact, it provides a Dirac-type pulse when the blade tip passes in front of it. The probe provides one pulse per revolution, corresponding to the passage of the vibrating blade. Figure 4.1 shows the Signal of a single sensor for a simulation performed over 30 revolutions. In parallel, the graph shows the pulses corresponding to the blade's passage with and without vibration in the front of the sensor. Hence, it is possible to observe 30 pulses corresponding to the passage of the blade with vibration in front of the sensor and 30 pulses corresponding to the blade's passage in front of the sensor without vibration.

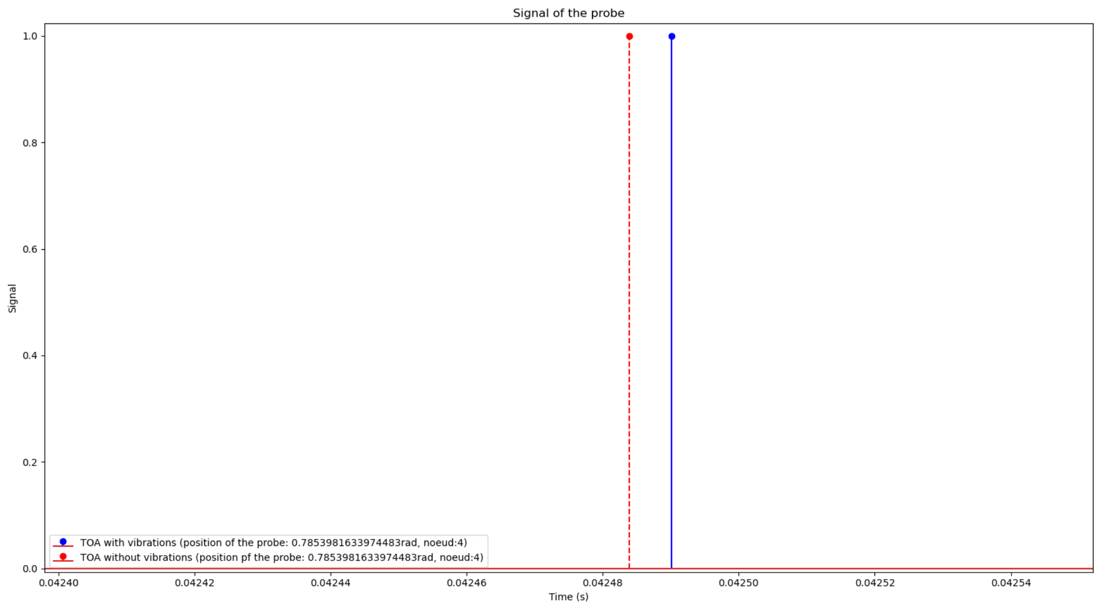

Figure 4.2. Magnification of the sensor signal of figure 4.1

4.2 Influence of simulation time step on TOA

TOA may be error-prone due to the following factors:

1. Inappropriate choice of simulation time step

2. Synchronous vibrations

Regarding the first cause, the error occurs if a lower dt than the difference of TOAs is not chosen. In practice, due to the time discretization principle, a permanent error is inherently present during the computation of the passage times. The maximum value is of the order of the time step. In particular, this error occurs when the TOA measurement is within an interval that has the same length as the dt so that the value of the measurement is approximated to the upper bound of that interval.

On the other hand, it is possible for another error to occur if the blade is excited at excitation frequencies corresponding to synchronous vibrations. Figure 4.3 shows the evolution of TOA as a function of time for an impeller rotation frequency of 215 Hz and a blade excitation frequency of 645 Hz; thus $EO = 3$ and $dt = 1e - 7$ $[sec]$ a slight saw-tooth periodicity of TOA difference can be seen.

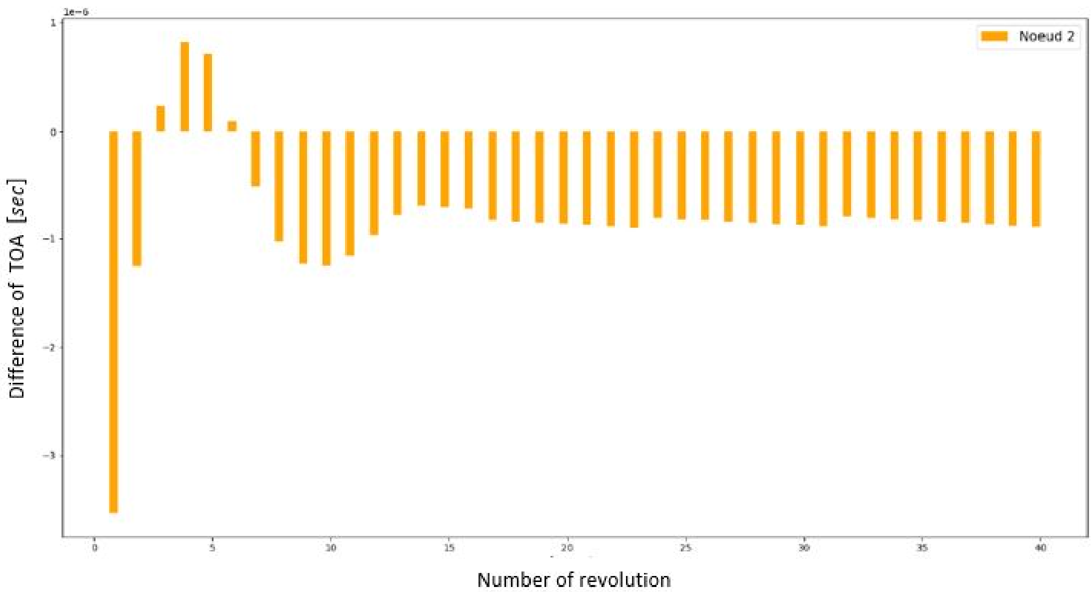

Figure 4.3. Difference in TOA as a function of the number of revolutions

This trend can be explained by reasoning about the pattern presented in figure 4.4

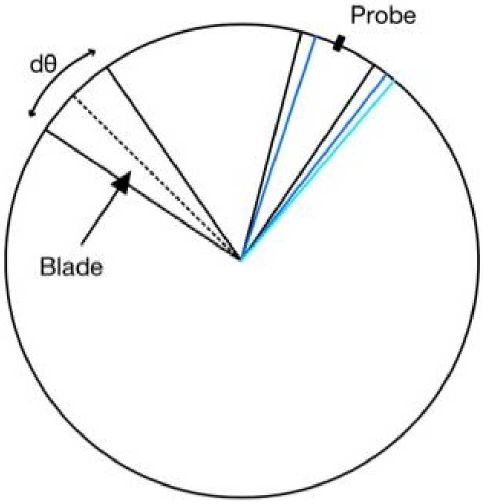

Figure 4.4.   Error in TOA Computation

More precisely, as pointed out above, for a blade passage in front of the probe in the time interval $[ndt, (n{+}1)dt]$ where $n \in N$ and dt is the time step of the simulation, represented by the angular step in black in the figure 4.4, the numerical TOA is approximated to $(n+1)dt$, which corresponds to the angular position $(n+1)d\theta$.

If this approximation is added to the presence of synchronous vibrations, we will consequently have the following behavior:

1. First measurement is represented in black in the figure
2. The next lap is not exactly in a time interval with the same angular position as the previous one, represented in blue It is slightly shifted
3. Proceeding with successive revolutions, the angular position of the new time step will be increasingly shifted, represented in light blue

As highlighted, because the vibrations are synchronous and the time taken by the blade to complete a revolution is not an integer multiple of the chosen time step, the measurement at the next revolution is not precisely in the same time frame as the previous one, so the next revolution is not precisely in a time interval with the same angular position as the previous one. Since TOAs are systematically approximated at the upper limit of the time interval the measurement is made, they increase with each new turn. As a result, the angular position of the measurement interval increases until the lower limit's angular position is greater than the sensor's. When this happens, the angular position of the time interval becomes the same as the initial one, and the cycle begins again. This explains the saw-tooth shape of the TOA difference in figure 4.3.

Given preventing this periodicity from occurring, as a first approximation, the simulation dt was opportunely chosen: Also, in this instance, the figure 4.5 shows the evolution of the TOA difference as a function of the number of revolutions, but in this case, for the same rotational frequency of the impeller thus 1350 rad/s, the chosen time step is $dt = 9.999809424e - 8$ $[sec]$, which allows an integer number of time steps during one revolution of the assembly. This time, the difference in TOA is effectively constant during the steady state.

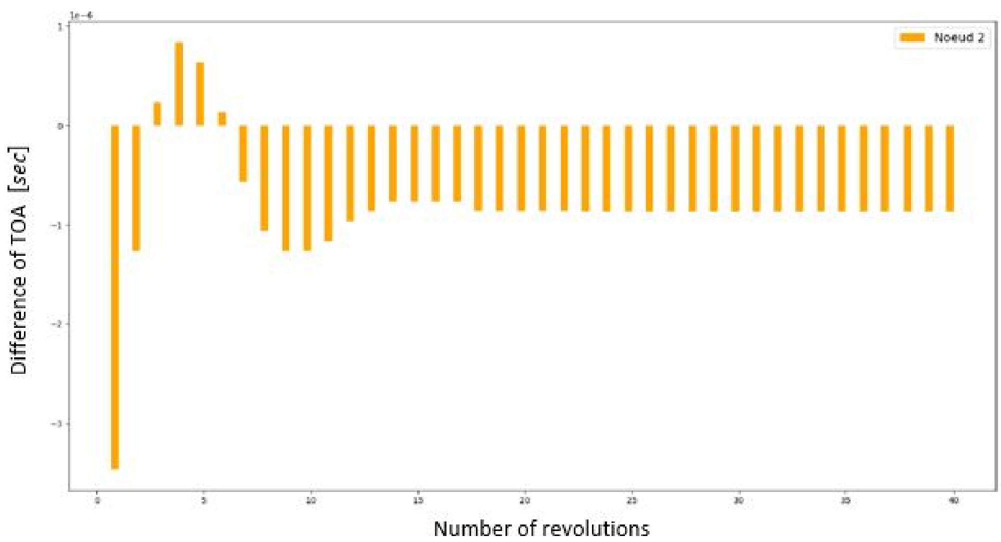

Figure 4.5. Appropriate choice of simulation time step

Subsequently, for better optimization of the algorithm, it was decided to generalize the code so that the simulation dt could be chosen with greater freedom, avoiding TOA measurement errors.

4.3 Improvement of computed Time of Arrival

In this context, the values of TOA approximated to the upper and lower bounds of the interval $[ndt, (n+1)dt]$ were computed. Once obtained, a linear interpolation between them was performed.

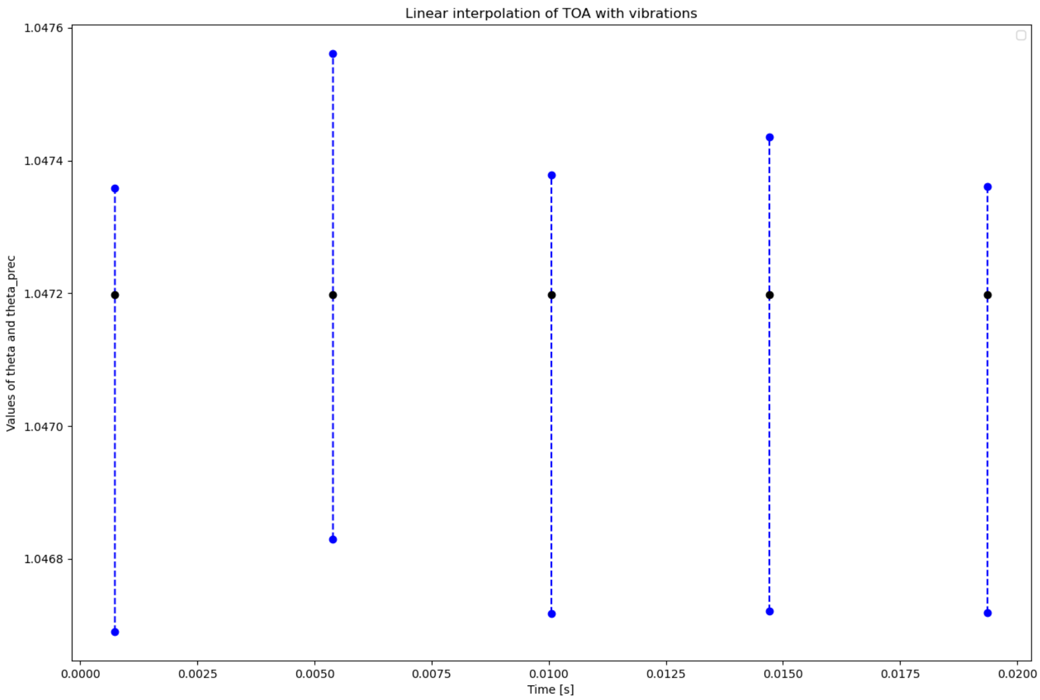

Figure 4.6. Linear interpolation of TOA

Figure 4.7 shows an example of a simulation in which it is visible how TOA was calculated:

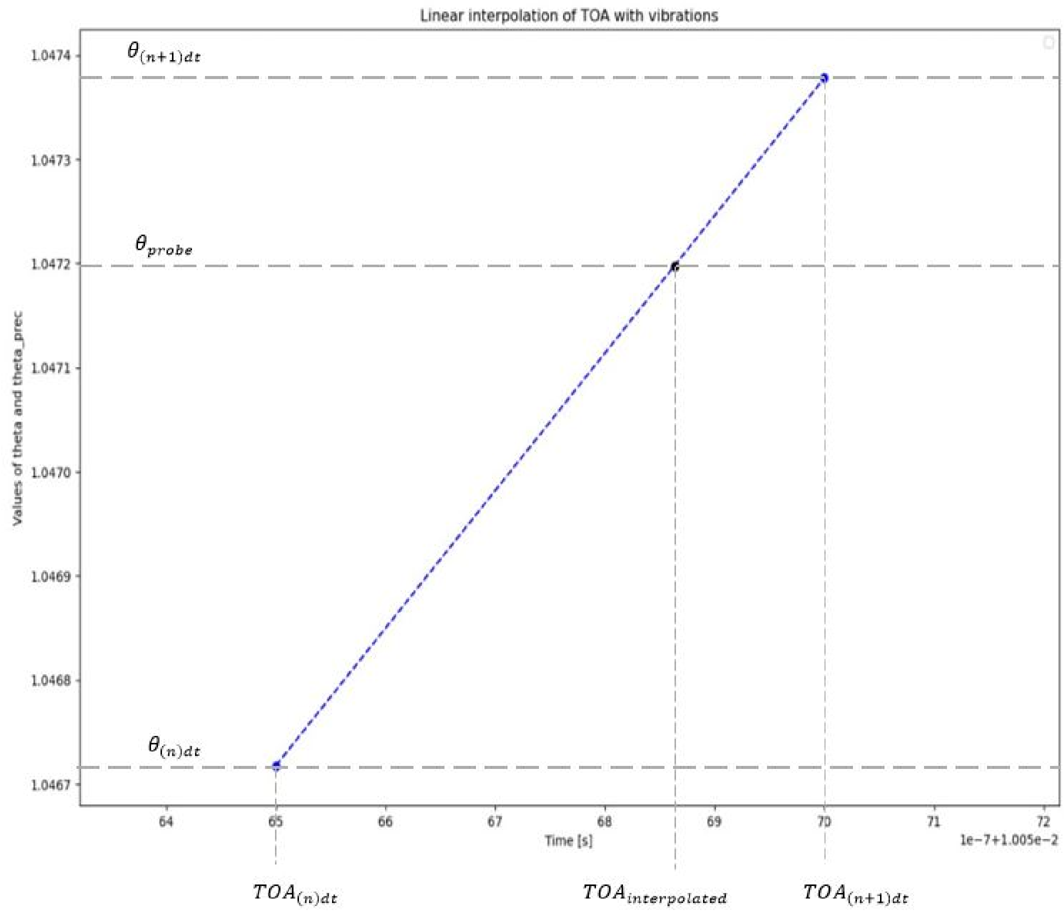

Figure 4.7. Magnification of the linear interpolation of TOA

4.4 Signal reconstruction

Upon obtaining the difference in TOA between the case with and without vibrations via equation 2.5, illustrated in the chapter on literature references 2, the corresponding measured amplitudes can be deduced. The case of synchronous vibration is considered, so keeping the rotation speed of the blade disk at 1350 $[rad/sec]$, the excitation frequency corresponding to $EO = 3$ is set. 3 unevenly distributed sensors are placed in $(\frac{\pi}{4}, \frac{\pi}{3}, \frac{pi}{2})$ and amplitude is measured from each of the sensors. These will differ from each other as sensors are placed non-uniformly on the casing;

by exploiting the equation, it is possible to obtain a system of 3 equations in three unknowns:

- $A \rightarrow$ maximum amplitude
- $\Omega \rightarrow$ the rotational speed of the assembly
- $\phi \rightarrow$ phase

$$\begin{cases} a_1 = A \sin\left(\omega t_{1,v} + \phi\right) \\ a_2 = A \sin\left(\omega t_{2,v} + \phi\right) \\ a_3 = A \sin\left(\omega t_{3,v} + \phi\right) \end{cases} \tag{4.1}$$

where $t_{p,v}$ corresponds to the TOA for a given revolution.

Because of the synchronous nature of the vibrations, the passage times in front of the sensor are almost uniformly spaced in time, which means that the measured amplitudes corresponding to the passage times are also almost constant with the number of revolutions. Therefore, the measured amplitudes are averaged by the lap corresponding to 65 % of the simulation time. Therefore, the steady state is assumed to have been reached. Since this system of equations is nonlinear, the system is solved numerically by searching for the roots of the function.

It is possible to summarize the process for The blade tip amplitude reconstruction, which consists of the following steps:

1. generation of the blade tip arrival time with and without vibration
2. Synchronization of the arrival time with the arrival time of the first blade without vibration captured by the first probe
3. calculation of the blade tip amplitude captured by the probe using equation 2.5
4. reconstruction of the maximum blade tip amplitude and the phase using the system of equations 4.1

Chapter 5

Simulation results

This chapter contains analyses performed to test the effectiveness of the proposed algorithms.

5.1 Influence of sensor position

Two cases were distinguished for this type of analysis.

5.1.1 Synchronous vibrations

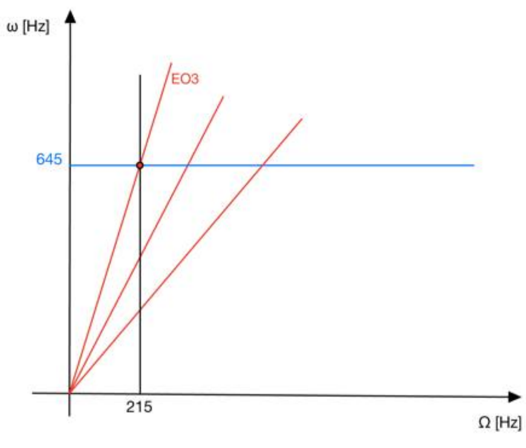

Figure 5.1. Campbell diagram for Synchronous vibrations

As the Campbell diagram shows in figure 5.1, the intersection between the two lines demonstrates the excitation of Engine Order 3 due to the chosen excitation frequency.

Table 5.1. Synchronous vibrations parameters

Synchronous vibrations			
Rotation speed	Ω	ω	EO
1350 $[rad/sec]$	215 $[Hz]$	645 $[Hz]$	3

Assuming that the evolution of TOA as a function of the number of revolutions has the same trend as the evolution of blade tangential displacement as a function of time, in this first case, the results in the figure 5.2 show the evolution, precisely of the difference in TOA, as a function of the angular position of the sensor. First, the difference in TOA is well proportional to the amplitude of the tangential displacement of the blade, figure 5.3, particularly with higher in the first seven revolutions, corresponding to the amplitude of the transient regime.

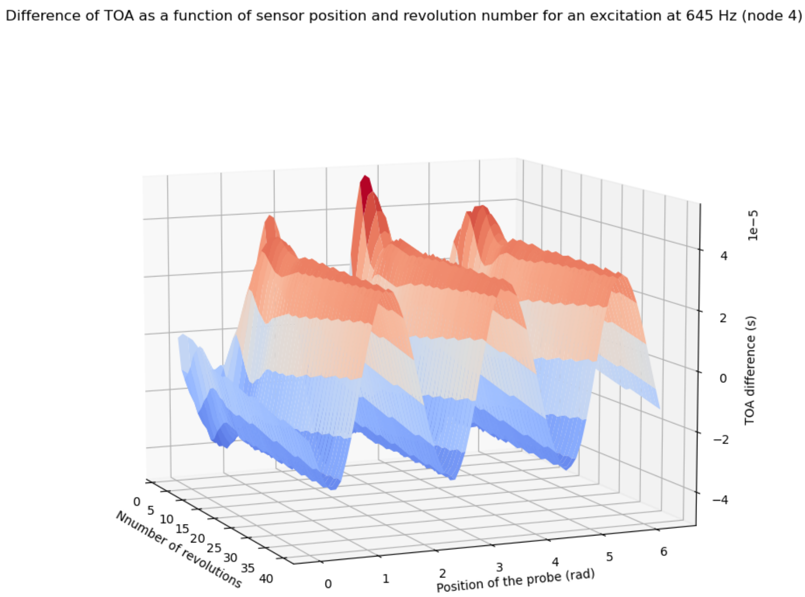

Figure 5.2. Difference in TOA as a function of speed and sensor position, in the case of synchronous vibration

The fact that we are in the presence of synchronous vibrations can be seen in figure 5.2, where the TOA difference, once the steady state is reached, is constant regardless of the number of revolutions. Moreover, this evolves periodically, with three periods visible in an interval of $[0,2\pi]$ that includes the angular position of the sensor. This last observation is also consistent with the excitation of the $EO = 3$.

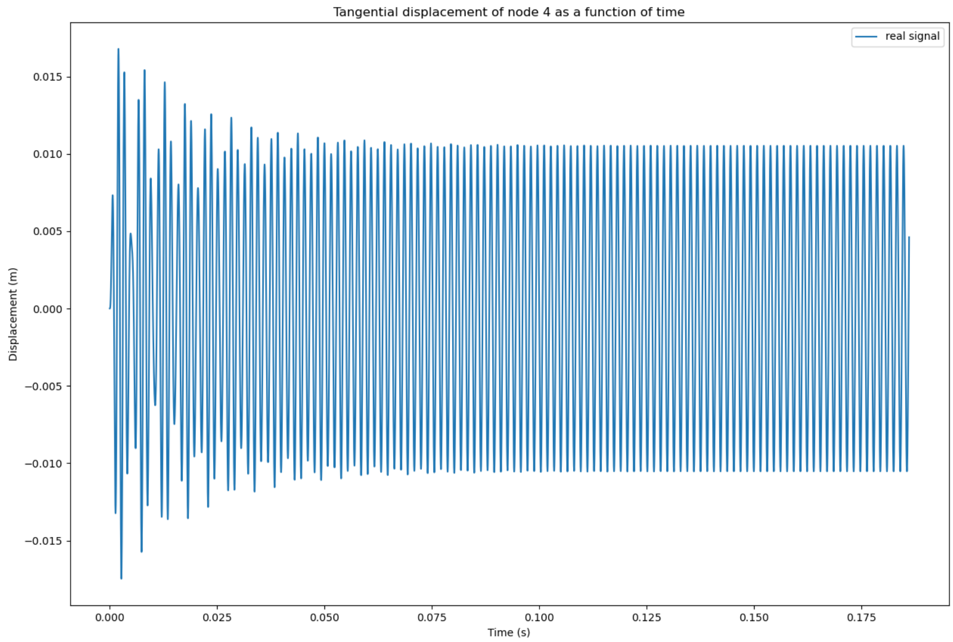

Figure 5.3. Tangential displacement of blade tip as a function of time, in the case of synchronous vibration

5.1.2 Asynchronous vibrations

Also, in this case, thanks to the Campbell diagram in figure 5.4, we can observe that since there is no intersection between the blade frequency curves and the exciting one, no particular Engine Order is excited.

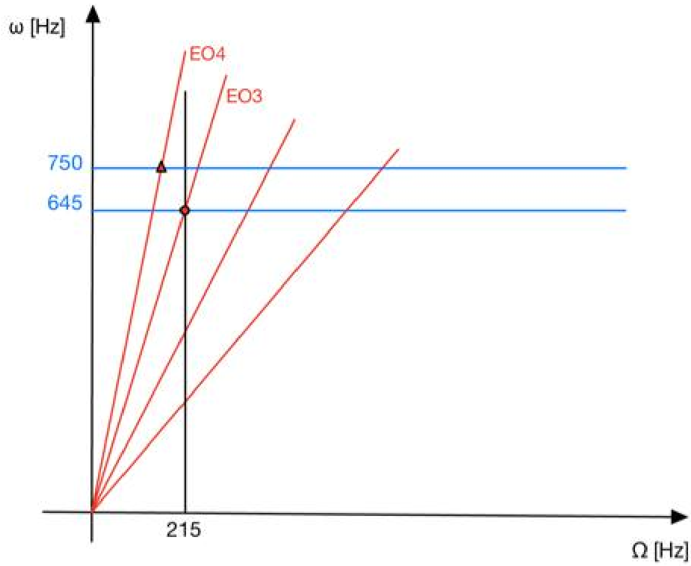

Figure 5.4. Campbell diagram for Asynchronous vibrations

In effect, as we saw in the previous case, to have an $EO = 3$, it is necessary to have an excitation frequency of 645 $[Hz]$, and similarly, for $EO = 4$, it would have to 860 $[Hz]$.

Table 5.2. Asynchronous vibrations parameters

Asynchronous vibrations			
Rotation speed	Ω	ω	EO
1350 $[rad/sec]$	215 $[Hz]$	750 $[Hz]$	X

As shown in the figure, again, the TOA difference is always proportional to the tangential vibration amplitude of the blade, figure. The non-constant trend can see Asynchronous vibrations of TOA difference as a function of revolutions.

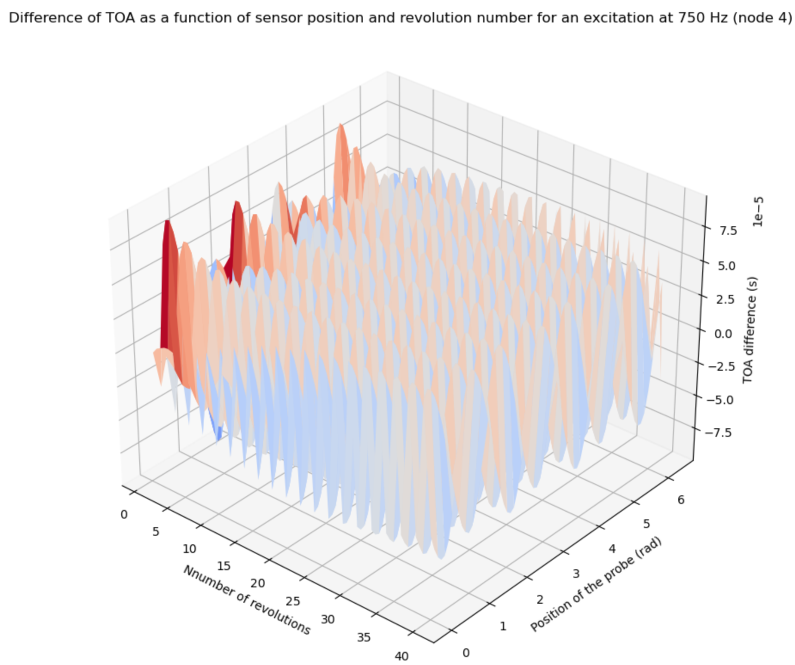

Figure 5.5. Difference in TOA as a function of speed and sensor position, in the case of asynchronous vibration

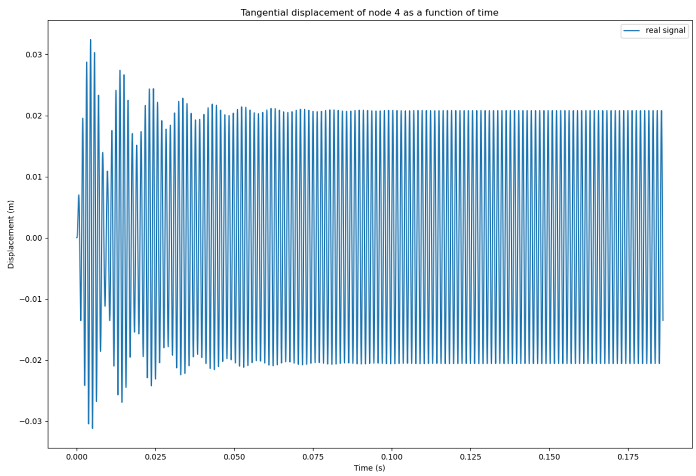

Figure 5.6. Tangential displacement of blade tip as a function of time, in the case of asynchronous vibration

5.2 Different TOA evaluated for a series of time steps

As mentioned in chapter 4, depending on how the TOA is calculated with vibrations, it may or may not be subject to some errors, which may be more or less relevant depending on the type of vibratory situation to be simulated.

In this regard, analyses to which different input parameters were given are presented below to verify the validity of the interpolation algorithm implemented to avoid the incumbency of such errors.

5.2.1 First analysis characteristics

- **Model**
  - single blade
  - 8 boundary nodes
- **Probe characteristics**
  - single probe
  - probe position at $\frac{\pi}{3}$
- **Forcing characteristics**
  - amplitude set equal to 0.0010
  - frequency set equal to 750 $[Hz]$
- **Simulation characteristics**
  - number of revolutions set equal to 5
  - rotational speed set equal to 1350 $[rad/sec]$
  - casing deformation set equal to 0
  - time steps used: $dt = 5e-8, 1e-8, 5e-7, 2.5e-7, 1e-7$ $[sec]$

Table 5.3. First analysis Data

First Tour Data			
Simulation time steps	$TOA_{(n+1)dt}$	$TOA_{interpolated}$	$TOA_{(n)dt}$
5.00E-08	0.000788	0.00078798	0.00078775
1.00E-08	0.000788	0.00078798	0.00078795
5.00E-07	0.00079	0.00078799	0.0007875
2.50E-07	0.00078875	0.00078799	0.0007875
1.00E-07	0.000788	0.00078798	0.0007875
Second Tour Data			
5.00E-08	0.00543725	0.00543711	0.005437
1.00E-08	0.00543715	0.00543712	0.0054371
5.00E-07	0.0054375	0.00543708	0.005435
2.50E-07	0.0054375	0.0054371	0.00543625
1.00E-07	0.0054375	0.00543711	0.005437
Third Tour Data			
5.00E-08	0.0101035	0.01010337	0.01010325
1.00E-08	0.0101034	0.01010338	0.01010335
5.00E-07	0.010105	0.01010337	0.0101025
2.50E-07	0.01010375	0.01010337	0.0101025
1.00E-07	0.0101035	0.01010337	0.010103
Fourth Tour Data			
5.00E-08	0.01475425	0.01475414	0.014754
1.00E-08	0.01475415	0.01475415	0.0147541
5.00E-07	0.014755	0.01475411	0.0147525
2.50E-07	0.014755	0.01475413	0.01475375
1.00E-07	0.0147545	0.01475413	0.014754
Fifth Tour Data			
5.00E-08	0.01941725	0.01941713	0.019417
1.00E-08	0.01941715	0.01941714	0.0194171
5.00E-07	0.0194175	0.01941715	0.019415
2.50E-07	0.0194175	0.01941714	0.01941625
1.00E-07	0.0194175	0.01941714	0.019417

First analysis plots

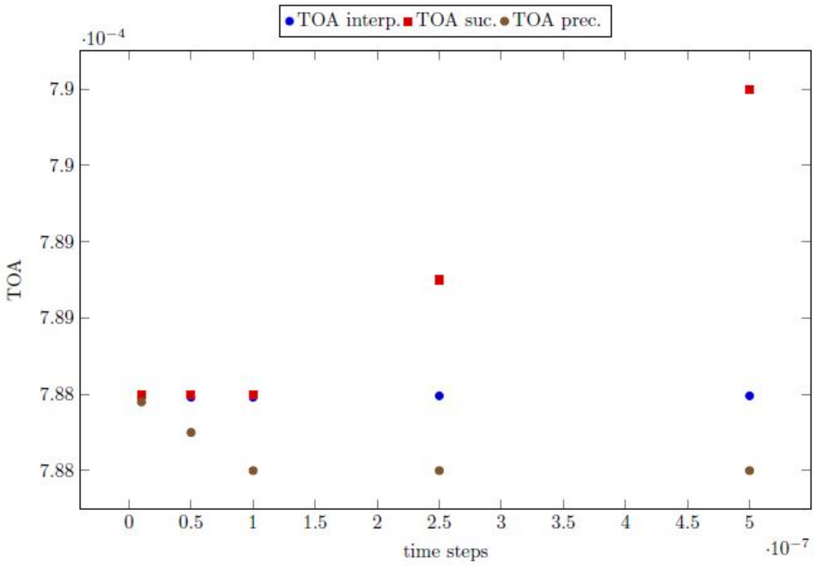

Figure 5.7. First Analysis: lap 1

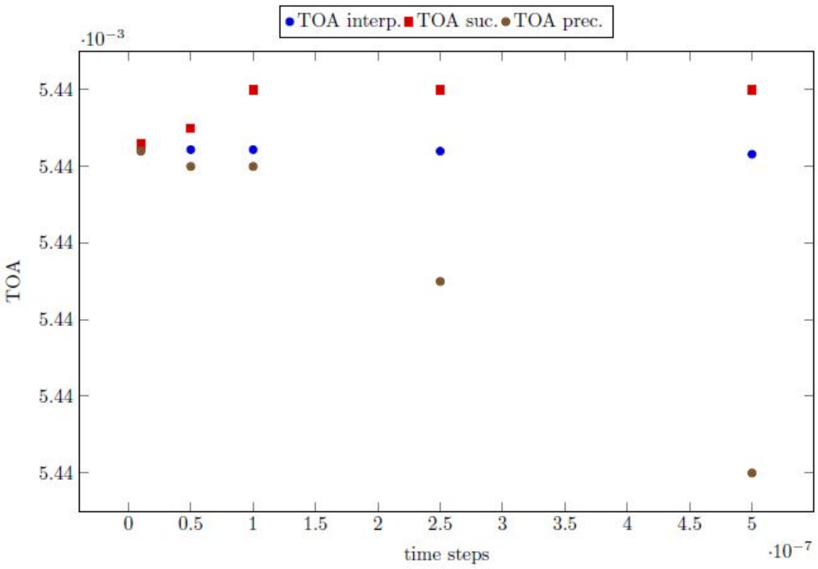

Figure 5.8. First Analysis: lap 2

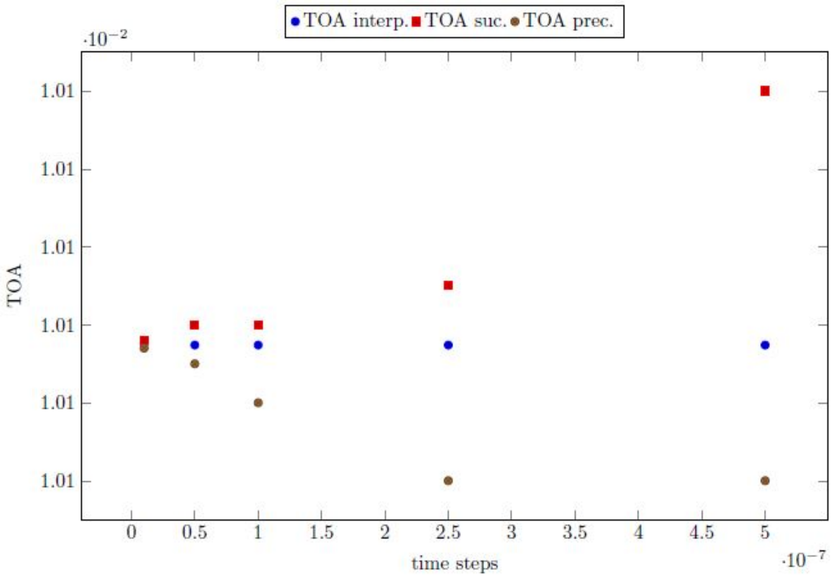

Figure 5.9. First Analysis: lap 3

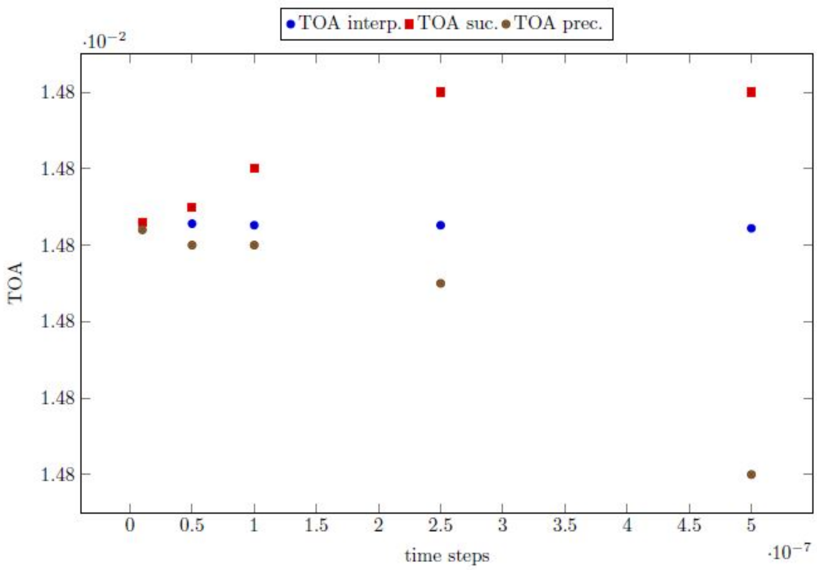

Figure 5.10. First Analysis: lap 4

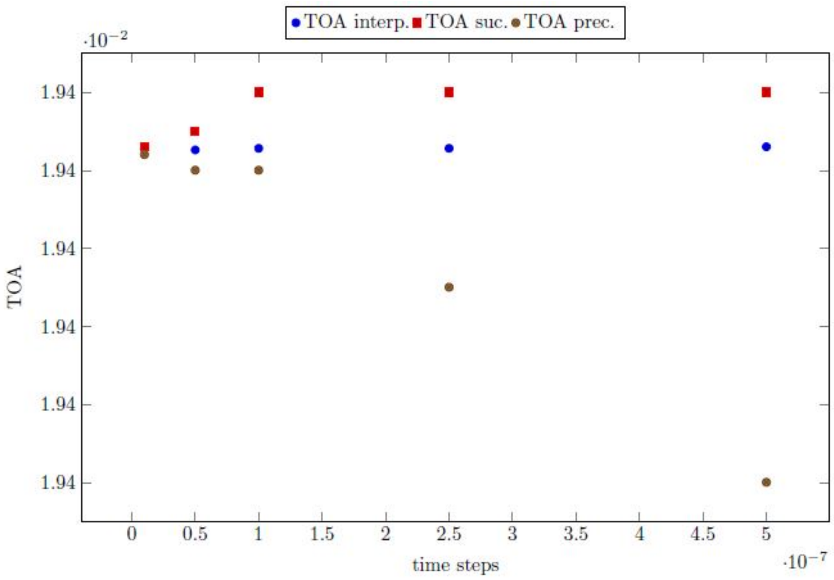

Figure 5.11. First Analysis: lap 5

The results highlight how linear interpolation is sufficient to eliminate restrictions on the choice of the simulation time step. While in the cases approximated by the chosen *dt*, the TOA values have significant variations, the interpretation is almost invisible by applying interpolation.

5.2.2 Second analysis characteristics

- **Model**
  - single blade
  - 8 boundary nodes
- **Probe characteristics**
  - single probe
  - probe position at $\frac{\pi}{3}$
- **Forcing characteristics**
  - amplitude set equal to 0.0010
  - frequency set equal to 750 $[Hz]$
- **Simulation characteristics**
  - number of revolutions set equal to 5
  - rotational speed set equal to 1350 $[rad/sec]$
  - casing deformation set equal to $1.2 * 5e - 3$
  - time steps used: $dt = 5e - 8, 1e - 8, 5e - 7, 2.5e - 7, 1e - 7$ $[sec]$

As previously reported, a correlation between tangential displacement trends and TOA has been established. TOA values were calculated for various simulations, each with a different time step dt. The resulting outputs were superimposed, and the displacements were found to overlap between simulations perfectly. However, in the last revolution 5.16, a trend was observed that did not conform with the previous ones, despite the values reported in the table appearing to align with the research. This discrepancy was found to be due to a purely numerical error, as demonstrated by Figure 5.17. It is important to note that interpolation is an approximation method, and while the results, in this case, show sufficient accuracy, it is possible to encounter errors due to numerical approximations.

Table 5.4. Second analysis Data

First Tour Data			
Simulation time steps	$TOA_{(n+1)dt}$	$TOA_{interpolated}$	$TOA_{(n)dt}$
5.00E-08	0.000788	0.00078798	0.00078775
1.00E-08	0.000788	0.00078798	0.00078795
5.00E-07	0.00079	0.00078799	0.0007875
2.50E-07	0.00078875	0.00078799	0.0007875
1.00E-07	0.000788	0.00078798	0.0007875
Second Tour Data			
5.00E-08	0.00543725	0.00543711	0.005437
1.00E-08	0.00543715	0.00543712	0.0054371
5.00E-07	0.0054375	0.00543708	0.005435
2.50E-07	0.0054375	0.0054371	0.00543625
1.00E-07	0.0054375	0.00543711	0.005437
Third Tour Data			
5.00E-08	0.010098	0.01009784	0.01009775
1.00E-08	0.01009785	0.01009785	0.0100978
5.00E-07	0.0101	0.01009776	0.0100975
2.50E-07	0.01009875	0.0100978	0.0100975
1.00E-07	0.010098	0.01009783	0.0100975
Fourth Tour Data			
5.00E-08	0.014736	0.01473579	0.01473575
1.00E-08	0.01473585	0.01473582	0.0147358
5.00E-07	0.0147375	0.01473551	0.014735
2.50E-07	0.01473625	0.01473567	0.014735
1.00E-07	0.014736	0.01473576	0.0147355
Fifth Tour Data			
5.00E-08	0.01936625	0.01936618	0.019366
1.00E-08	0.0193651	0.01936508	0.01936505
5.00E-07	0.0193575	0.0193571	0.019355
2.50E-07	0.0193625	0.01936173	0.01936125
1.00E-07	0.0193675	0.01936727	0.019367

Second analysis plots

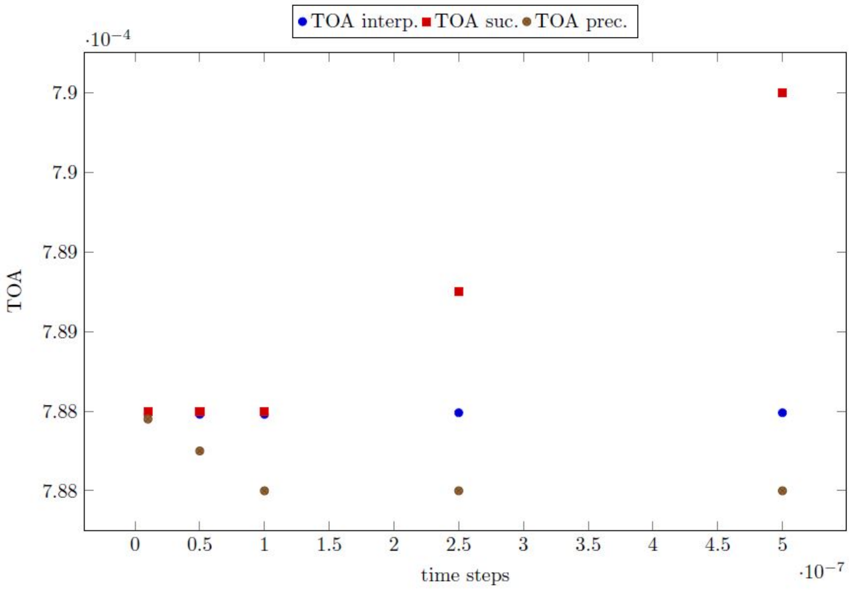

Figure 5.12. Second Analysis: lap 1

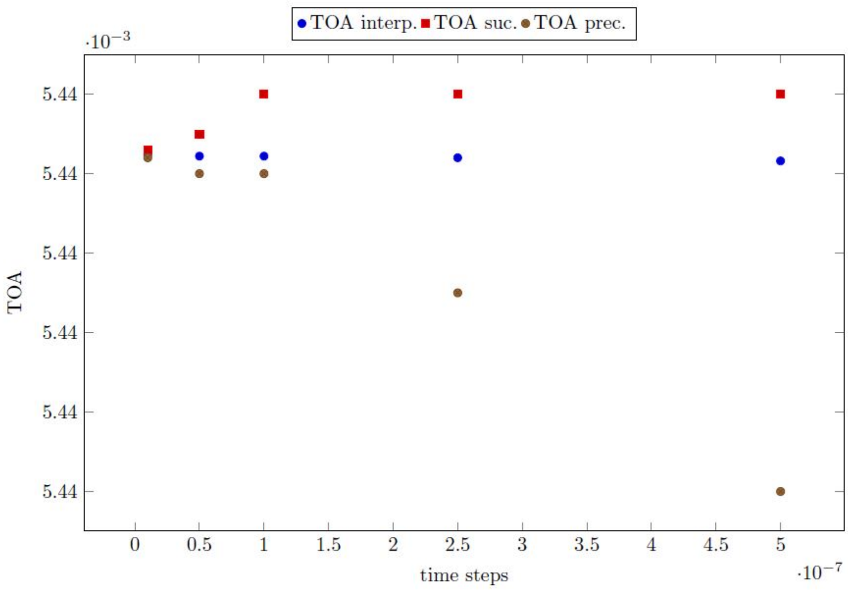

Figure 5.13. Second Analysis: lap 2

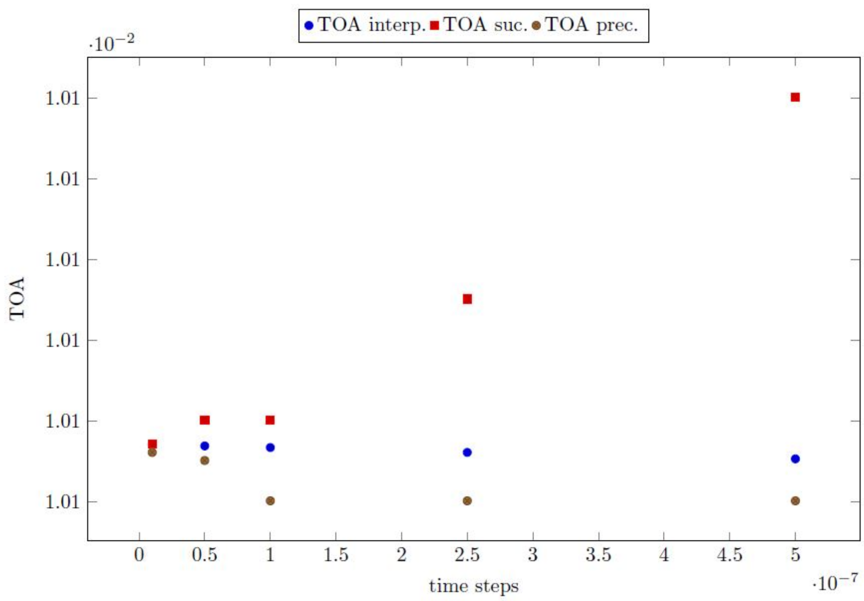

Figure 5.14. Second Analysis: lap 3

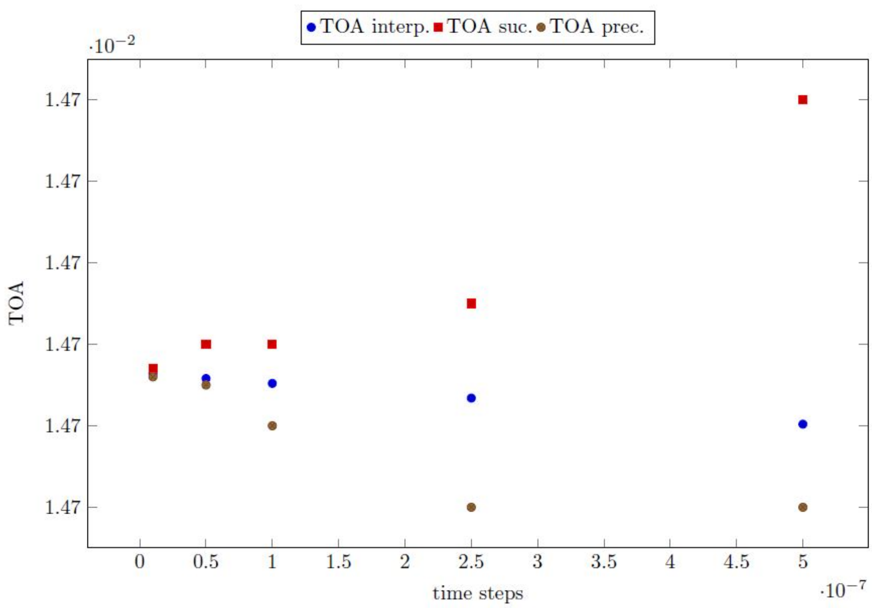

Figure 5.15. Second Analysis: lap 4

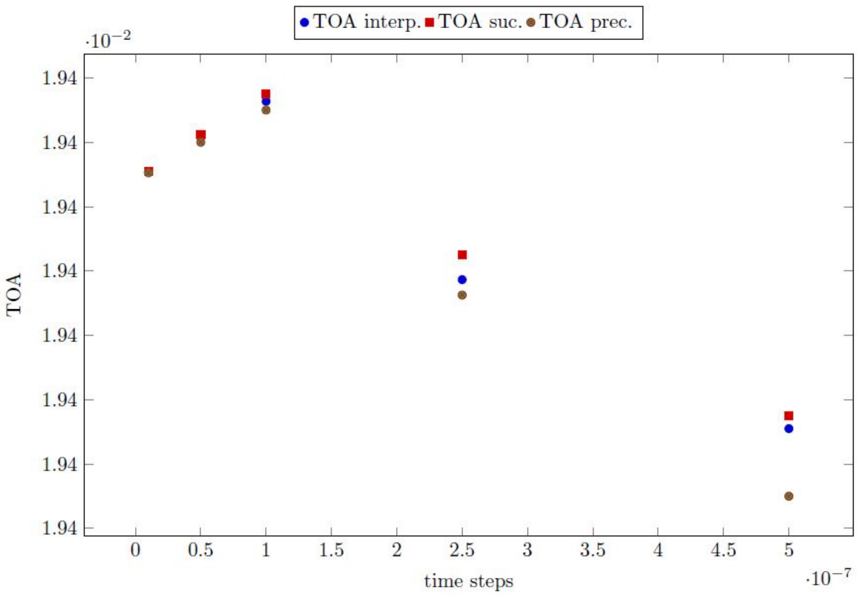

Figure 5.16. Second Analysis: lap 5

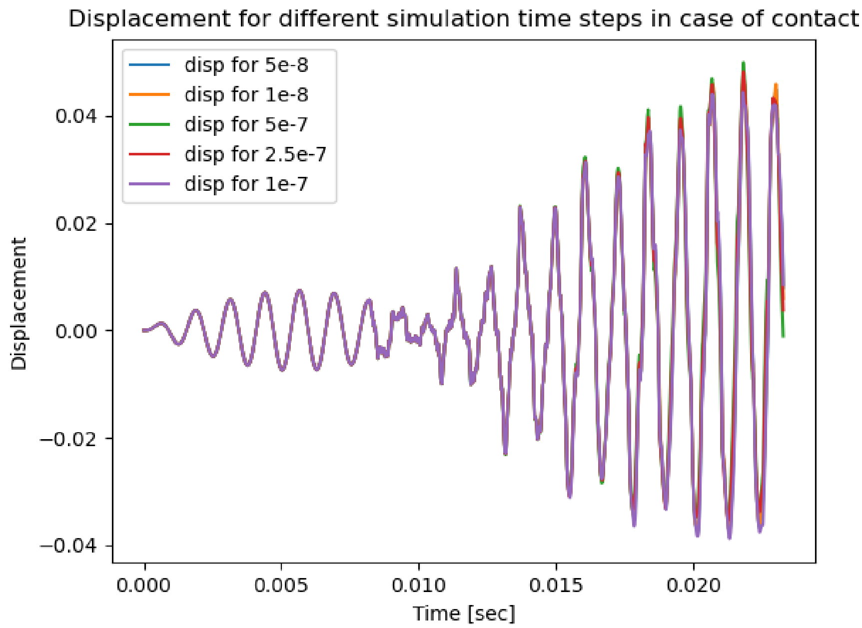

Figure 5.17. Convergence concerning time

5.3 Signal reconstruction

We have seen in chapter 4 how the signal reconstruction is done numerically. The reconstructed signal, shown in the figures 5.18 and 5.19, is extremely close to the original signal once the steady state is reached. The slight differences in amplitude and frequency, compounded by a slight phase shift, are due to the approximation of run times during time integration. In addition, the module for solving the system of equations, which is equivalent to determining the roots of an equation, is also subject to approximations.

Although these approximations are very small and the signal reconstruction method is very satisfactory in the case shown, following the improvement in the computation of TOA by the interpolation algorithm, the figures 5.20 and 5.21, illustrate how the real signal and that reconstructed through BTT, reveal differences but are much more similar than the previous case.

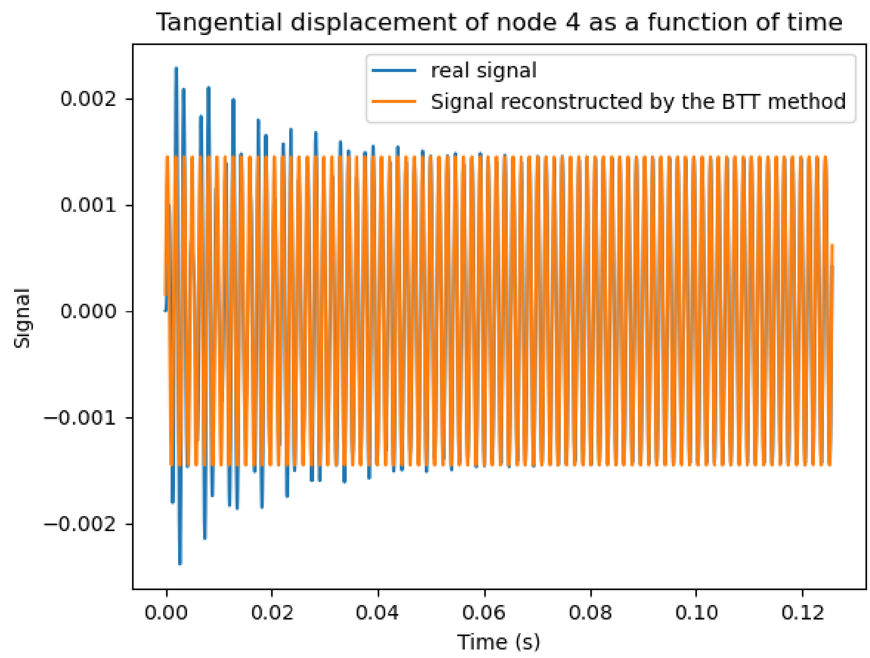

Figure 5.18. Tangential displacement of node four versus time

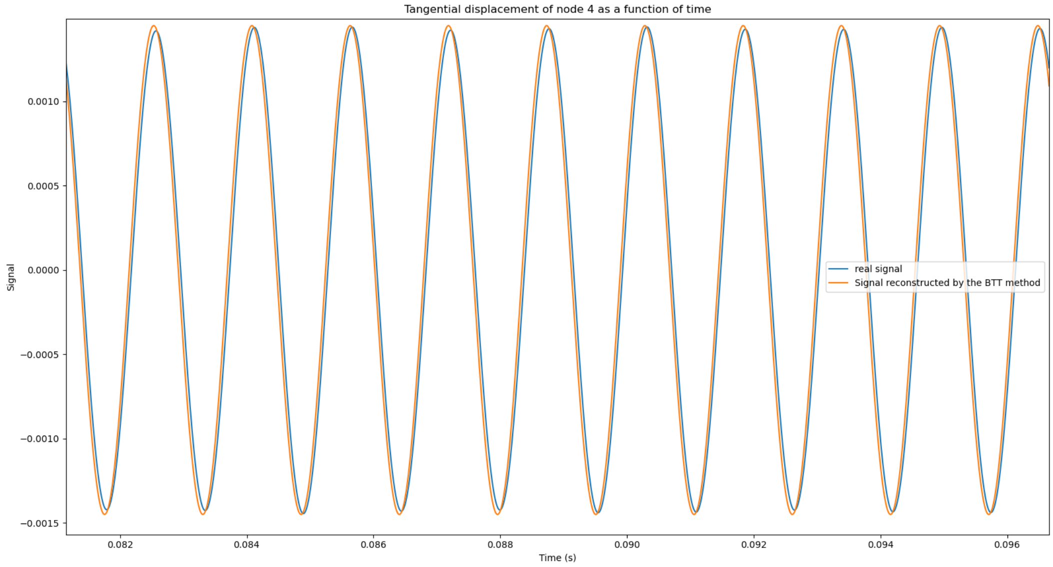

Figure 5.19. Magnification of tangential displacement of node four versus time

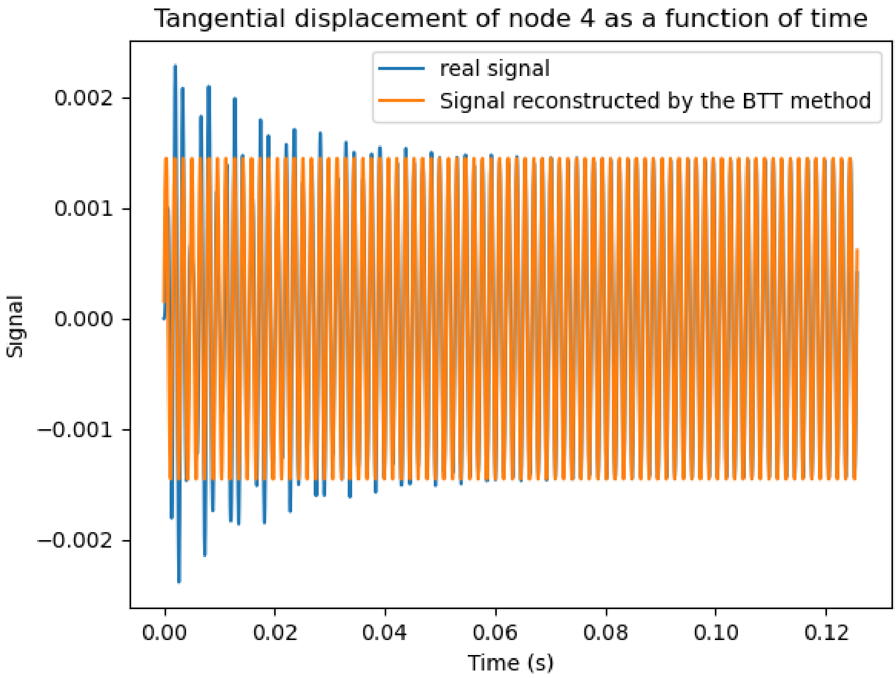

Figure 5.20. Tangential displacement versus time using $TOA_{interpolated}$

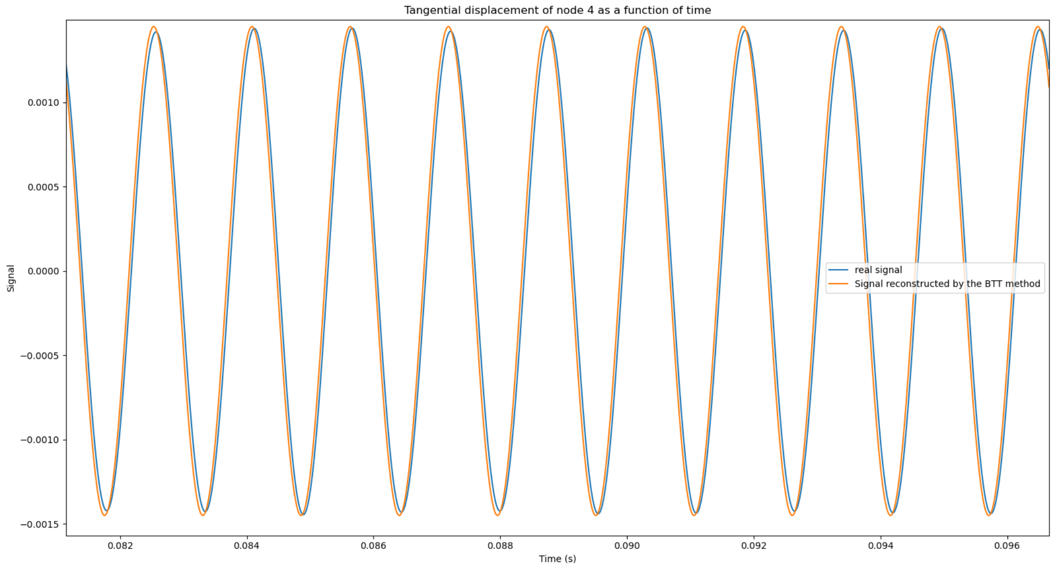

Figure 5.21. Magnification of tangential displacement using $TOA_{interpolated}$

Chapter 6

Conclusions

6.1 Summary of Project

This thesis project successfully developed a Python code that generates blade tip-timing signals. The single-blade model used in this project simulated linear and sinusoidal vibrations, and the times of arrival obtained were consistent with changes in angular positions and excitation parameters. The TOA allowed for identifying blade frequencies and deducing corresponding vibration amplitudes without mistuning. Additionally, the technique for reconstructing the vibration signal was effective for linear and sinusoidal vibrations.

6.2 Limitations of Proposed Solution

The BTT signals were generated based on a single-blade model without considering the mistuning in real-bladed disks. However, the generated signals were independent of the fan model and can be used for other models. Unfortunately, the reconstruction technique cannot be applied to mistuned bladed-disk models, and the digital measurements do not account for experimental noise.

6.3 Future Improvements

To improve the fidelity of the measurements, the numerical code can be enhanced to reproduce experimental noise, such as random noise introduced in the positioning of sensors. The pulse signal of the digital sensor can also be adapted based on the sensor's response to blade passage. Additionally, further developments can be made to study the characteristics of different TOA and reconstruct signals for non-linear vibrations, especially during blade-casing contacts.

Bibliography

[1] MachineDesign, "What's the Difference Between Turbine Engines," 2016.

[2] E. Piollet, F. Nyssen, and A. Batailly, "Blade/casing rubbing interactions in aircraft engines: Numerical benchmark and design guidelines based on nasa rotor 37," *Journal of Sound and Vibration*, vol. 460, no. 4, p. 114878, 2019.

[3] S. Bornassi, T. Berruti, C. Firrone, and G. Battiato., "Vibration parameters identification of turbomachinery rotor blades under transient condition using blade tip-timing measurements," *Measurement*, vol. 183, p. 109861, 2021.

[4] M. Pan, Y. Yang, F. Guan, H. Hu, and H. Xu., "Sparse representation based frequency detection and uncertainty reduction in blade tip timing measurement for multi-mode blade vibration monitoring," *Sensors*, vol. 17(8), p. 1745, 2017.

[5] "Sampling signals." https://www.ni.com/docs/en-US/bundle/labview/page/lvanlsconcepts/aliasing.html. Updated: 2023-02-23.

[6] Heath and Steve, "A New Technique for Identifying Synchronous Resonances Using Tip-Timing ," *Journal of Engineering for Gas Turbines and Power*, vol. 122, no. 2, pp. 219–225, 2000.

[7] "D. hubler, rotor 37 and stator 37 assembly (series: Photographs relating to agency activities, facilities and personnel, 1973 - 2013), 1977." https://catalog.archives.gov/id/17468361.

[8] J. Joachim, "Développement de modèles numériques de roues aubagées désaccordées dans un contexte non-linéaire.," PhD thesis, Ecole Polytechnique de Montréal, 2020.

[9] O. Jousselin, "Development of blade tip timing techniques in turbo machinery," *Turbo Machinery, PhD thesis, 2013*.

[10] S. Heath and M. Imregun., "A review of analysis techniques for blade tip-timing measurements," *Turbo Expo : Power for Land, Sea, and Air*, vol. 78712, p. V004T15A016, 1997.

[11] Y. Colaïtis, "Stratégie numérique pour l'analyse qualitative des interactions aube/carter," 2021. PhD thesis, École Polytechnique de Montréal.

[12] G. Rigosi, G. Battiato, and T. M. Berruti, "Synchronous vibration parameters identification by tip timing measurements," *Mechanics Research Communications*,

vol. 79, pp. 7–14, 2017.

[13] Kharyton, V, Dimitriadis, , and Defise, "A discussion on the advancement of blade tip timing data processing," *ASME Turbo Expo 2017: Turbomachinery Technical Conference and Exposition*, vol. 7B: Structures and Dynamics., pp. 7–14, 2017. https://doi.org/10.1115/GT2017-63138.

[14] D. D. M. end D. Ewins, "Experimental measurements of out-of-plane vibrations of a simple blisk design using blade tip timing and scanning ldv measurement methods," *Mechanical Systems and Signal Processing*, vol. 28, p. 517–527, 2012.

[15] S. Madhavan, R. Jain, C. Sujatha, and A. Sekhar, "Experimental investigation on forced response of mistuned bladed disc rotor in an aero-engine," *Journal of Aerospace Engineering*, vol. 229, p. 2572–2588, 2015.

[16] V. Kharyton, J.-P. Laine, F. Thouverez, and O. Kucher, "Simulation of tip-timing measurements of a cracked bladed disk forced response," *In Turbo Expo : Power for Land, Sea, and Air*, vol. 44014, p. 845–854, 2010.

[17] "Sensor basics." https://www.keyence.com/ss/products/sensor/sensorbasics/proximity/info/.

[18] J. Zhang, F. Duan, G. Niu, J. Jiang, and J. Li, "A blade tip timing method based on a microwave sensor ," *PhD Thesis, University of London - Imperial College London*, vol. 17, p. 1–11, 2017.

[19] N. Jamia, M. Friswell, S. El-Borgi, and R. Fernandes, "Simulating eddy current sensor outputs for blade tip timing," *Advances in Mechanical Engineering*, vol. 10, p. 168781401774802, 01 2018.

[20] N. Jamia[1] and M. I. F. . S. El-Borgi, "The effect of sensor characteristics on blade tip timing measurements," *College of Engineering, Swansea University, UK. Department of Mechanical Engineering, Texas AM University at Qatar, Qatar.*

[21] "Sample records for blade tip timing." https://www.science.gov/topicpages/b/blade+tip+timing.

[22] Georgiev, V., Holik, Michael, Kraus, Vaclav, Krutina, Aleš, Kubin, Zdenek, Liska, Jindrich, Poupa, and Martin, "The blade flutter measurement based on the blade tip timing method," pp. 270–275, 07 2011.

[23] Z. JW, Z. LB, and D. LX., "A blade defect diagnosis method by fusing blade tip timing and tip clearance information," *Sensors (Basel)*, 2018.

[24] F. Ken-ichi, J.-w. Zhang, K.-q. Ding, and G. Chen, "High-precision extraction method for blade tip-timing signal with eddy current sensor," *International Journal of Rotating Machinery*, 2020.

[25] J.-H. Cao, Z.-B. Yang, H.-Q. Li, G.-R. Teng, S.-H. Tian, W.-B. Li, , and X.-F. Chen., "Rotating blade frequency identification by single-probe blade tip timing.," *Mechanical Systems and Signal Processing*, vol. 172, p. 108961, 2022.

[26] Mishali, Moshe, Eldar, and Yonina, "Sub-nyquist sampling: Bridging theory and

practice," *IEEE Signal Processing Magazine*, vol. 28, 2011.

[27] V. Kharyton, C. Gibert, L. Blanc, and F. Thouverez, "Elements of dynamic characterization of a bladed disk by using the tip-timing method under vacuum conditions," *In Turbo Expo : Power for Land, Sea, and Air*, vol. 54662, p. 1127–1135, 2011.

[28] I. Y. Zablotskiy and Y. A. Korostelev, "Measurement of resonance vibrations of turbine blades with the elura device," *Energomashinostroneniye*, 1970.

[29] P. S. Zucca, *Dinamica dei rotori per applicazioni aerospaziali Laurea Magistrale in Ingegneria Aerospaziale.* 2021.

[30] S. Heath and M. Imregun, "An improved single-parameter tip-timing method for turbomachinery blade vibration measurements using optical laser probes ," *International Journal of Mechanical Sciences*, vol. 38, no. 10, p. 1047–1058, 1996.

[31] M. Nikpour, S. Moradi, and I. Soodmand, "A new bladed assembly simulator and an improved two-parameter plot method for blade tip-timing numerical simulations," *Proceedings of the Institution of Mechanical Engineers, Part G: Journal of Aerospace Engineering*, vol. 235, no. 14, pp. 2135–2144, 2021.

[32] Heath and Steven, "A study of tip-timing measurement techniques for the determination of bladed-disk vibration characteristics ," *PhD Thesis, University of London - Imperial College London*, 1997.